The Astrophysical Journal, 847:134 (21pp), 2017 October 1 https://doi.org/10.3847/1538-4357/aa8b75

Effect of Local Environment and Stellar Mass on Galaxy Quenching and Morphology at $0.5 < z < 2.0$*

Lalitwadee Kawinwanichakij[1,2,16], Casey Papovich[1,2], Ryan F. Quadri[1,2,17], Karl Glazebrook[3], Glenn G. Kacprzak[3], Rebecca J. Allen[3], Eric F. Bell[4], Darren J. Croton[3], Avishai Dekel[5], Henry C. Ferguson[6], Ben Forrest[1,2], Norman A. Grogin[6], Yicheng Guo[7], Dale D. Kocevski[8], Anton M. Koekemoer[6], Ivo Labbé[9], Ray A. Lucas[6], Themiya Nanayakkara[3,9], Lee R. Spitler[10,11,12], Caroline M. S. Straatman[13], Kim-Vy H. Tran[1,2], Adam Tomczak[14], and Pieter van Dokkum[15]

[1] Department of Physics and Astronomy, Texas A&M University, College Station, TX 77843-4242, USA; kawinwanichakij@physics.tamu.edu
[2] George P. and Cynthia Woods Mitchell Institute for Fundamental Physics and Astronomy, Texas A&M University, College Station, TX 77843-4242, USA
[3] Centre for Astrophysics and Supercomputing, Swinburne University, Hawthorn, VIC 3122, Australia
[4] Department of Astronomy, University of Michigan, 1085 South University Ave., Ann Arbor, MI 48109-1107, USA
[5] Racah Institute of Physics, The Hebrew University, Jerusalem 91904, Israel
[6] Space Telescope Science Institute, 3700 San Martin Drive, Baltimore, MD 21218, USA
[7] UCO/Lick Observatory, Department of Astronomy and Astrophysics, University of California, Santa Cruz, CA, USA
[8] Department of Physics and Astronomy, Colby College, Waterville, ME 04901, USA
[9] Leiden Observatory, Leiden University, P.O. Box 9513, 2300 RA Leiden, The Netherlands
[10] Australian Astronomical Observatory, P.O. Box 915, North Ryde, NSW 1670, Australia
[11] Research Centre for Astronomy, Astrophysics & Astrophotonics, Macquarie University, Sydney, NSW 2109, Australia
[12] Department of Physics & Astronomy, Macquarie University, Sydney, NSW 2109, Australia
[13] Max-Planck Institut für Astronomie, Königstuhl 17, D-69117, Heidelberg, Germany
[14] Department of Physics, UC Davis, Davis, CA 95616, USA
[15] Astronomy Department, Yale University, New Haven, CT 06511, USA
Received 2017 June 11; revised 2017 August 26; accepted 2017 September 8; published 2017 October 3

Abstract

We study galactic star formation activity as a function of environment and stellar mass over $0.5 < z < 2.0$ using the FourStar Galaxy Evolution (ZFOURGE) survey. We estimate the galaxy environment using a Bayesian-motivated measure of the distance to the third nearest neighbor for galaxies to the stellar mass completeness of our survey, $\log(M/M_{\odot}) > 9$ (9.5) at $z = 1.3$ (2.0). This method, when applied to a mock catalog with the photometric-redshift precision ($\sigma_z/(1+z) \lesssim 0.02$) of ZFOURGE, accurately recovers galaxies in low- and high-density environments. We quantify the environmental quenching efficiency and show that at $z > 0.5$, it depends on galaxy stellar mass, demonstrating that the effects of quenching related to (stellar) mass and environment are not separable. In high-density environments, the mass and environmental quenching efficiencies are comparable for massive galaxies ($\log(M/M_{\odot}) \gtrsim 10.5$) at all redshifts. For lower-mass galaxies ($\log(M/M)_{\odot}) \lesssim 10$), the environmental quenching efficiency is very low at $z \gtrsim 1.5$, but increases rapidly with decreasing redshift. Environmental quenching can account for nearly all quiescent lower-mass galaxies ($\log(M/M_{\odot}) \sim 9$–10), which appear primarily at $z \lesssim 1.0$. The morphologies of lower-mass quiescent galaxies are inconsistent with those expected of recently quenched star-forming galaxies. Some environmental process must transform the morphologies on similar timescales as the environmental quenching itself. The evolution of the environmental quenching favors models that combine gas starvation (as galaxies become satellites) with gas exhaustion through star formation and outflows ("overconsumption"), and additional processes such as galaxy interactions, tidal stripping, and disk fading to account for the morphological differences between the quiescent and star-forming galaxy populations.

Key words: galaxies: evolution – galaxies: groups: general – galaxies: high-redshift – galaxies: star formation

1. Introduction

The population of galaxies can be broadly classified into two distinct types: quiescent galaxies with relatively red colors, spheroid-dominated morphologies, and little to no ongoing star formation activity (with star formation rates, SFRs, much less than their past averages); and star-forming galaxies with relatively blue colors, disk-dominated morphologies, and SFRs comparable to (or above) their past averages (e.g., Strateva et al. 2001; Kauffmann et al. 2003; Baldry et al. 2004, 2006; Bell 2008; van Dokkum et al. 2011; Schawinski et al. 2014). In the local universe, it is well-known that these types of galaxies are related to the density of galaxies (the galaxy environment). Quiescent, spheroidal galaxies are preferentially found in dense environments rich with galaxies (e.g., Oemler 1974; Davis & Geller 1976; Dressler 1980; Balogh et al. 2004; Hogg et al. 2004; Kauffmann et al. 2004; Blanton & Moustakas 2009; Peng et al. 2010; Woo et al. 2013).

How this trend with environment manifests and evolves with redshift is one of the outstanding questions in galaxy evolution. Multiple studies have found a correlation between environmental density and the quenching of star formation at $z \sim 1$ (e.g., Cooper et al. 2007, 2010; Cucciati et al. 2010; Kovač et al. 2010, 2014; Muzzin et al. 2012; Allen et al. 2016; Balogh et al. 2016; Morishita et al. 2017; Guo et al. 2017). In addition, there is some observational evidence that the environment (or

* This paper includes data gathered with the 6.5 m Magellan Telescopes located at Las Campanas Observatory, Chile.
[16] LSSTC Data Science Fellow.
[17] Mitchell Astronomy Fellow.

by proxy, the density of galaxies) correlates with other galaxy properties out to $z \sim 2$ (e.g., Cucciati et al. 2006; Tran et al. 2010; Chuter et al. 2011; Papovich et al. 2012; Quadri et al. 2012; Fossati et al. 2017; Nantais et al. 2016), and possibly to at least $z \sim 3$ (Darvish et al. 2016). Developing a further understanding of the physical processes involved in the quenching of star formation clearly requires better observational measurements and also requires disentangling the observed correlations among SFR, galaxy structure, and environmental density out to these higher redshifts.

In the low-redshift universe ($z \lesssim 0.1$), it has been shown that the effect of the respective relationships between stellar mass and environment on quenching are largely separable (e.g., Baldry et al. 2006; van den Bosch et al. 2008; Peng et al. 2010; Kovač et al. 2014), implying that there are two distinct quenching processes at work: one that correlates with stellar mass (independent of environment) and one that correlates with galaxy environment (independent of stellar mass). Peng et al. (2010) show the separability of the effects of stellar mass and environment on the quiescent fraction of galaxies in SDSS (at $z < 0.1$) and zCOSMOS ($0.3 < z < 0.6$). Similarly, Kovač et al. (2014) used mass-matched samples of central and satellite galaxies to show that the quiescent fraction of centrals is primarily related to stellar mass and is almost independent of overdensity (environment), indicating that they are mainly quenched by a process related to stellar mass, at least to the stellar mass limit of their data ($\log M/M_{\odot} > 9.8$ at $z = 0.4$). On the other hand, an additional environmental quenching process is required to explain the observed quiescent fraction of satellite galaxies, which increases with galaxy overdensity.

These separable effects of stellar mass and environment on galaxy properties have been observed out to $z \sim 3$ (e.g., Quadri et al. 2012; Muzzin et al. 2012; Lee et al. 2015; Darvish et al. 2016), but have been limited to more massive galaxies, $\log M/M_{\odot} \gtrsim 10$, due to the depth of the surveys. To this mass limit, these studies also found no evidence that the properties of star-forming galaxies strongly depend on environment: there is no significant change in the median SFR and specific SFR (for star-forming galaxies) with environment at fixed stellar mass, suggesting that the independence of the SFR–mass sequence from the environment has been in place at $z \sim 3$ (but see Jian et al. 2017). The obvious qualifier is that it has only been possible to study the relatively higher-mass galaxies, and it is unknown if these results extend to lower-mass galaxies.

Physical explanations for the cessation of star formation in galaxies can also be broadly classified into mechanisms that are related to either mass (halo mass, supermassive black hole mass, or stellar mass) or the environment. A galaxy's halo mass provides a natural quenching mechanism related to mass (e.g., Rees & Ostriker 1977; White & Rees 1978; Gabor et al. 2011; Gabor & Davé 2015). It is generally argued that the intrahalo gas in halos above $\sim 10^{12} M_{\odot}$ exists at temperatures high enough (Birnboim & Dekel 2003; Kereš et al. 2005) to shock-heat infalling gas from the intergalactic medium at the virial radius, preventing the fueling of star formation in the galaxies (Cattaneo et al. 2006; Dekel & Birnboim 2006; Birnboim et al. 2007). Another quenching mechanism that may be related to galaxy mass is the feedback from an active galactic nucleus (AGN; Granato et al. 2004; Springel et al. 2005; Bower et al. 2006; Cattaneo et al. 2006; Croton et al. 2006; Somerville et al. 2008; Knobel et al. 2015; Terrazas et al. 2016). In contrast, the suppression of star formation in galaxies in low-mass halos can be driven by energetic feedback from supernova explosions and stellar winds (e.g., Larson 1974; Dekel & Silk 1986).

There are also physical processes that operate preferentially in dense environments. One of them is the rapid stripping of cold gas via ram pressure as the galaxy passes through a hot gaseous medium, causing abrupt quenching (Gunn & Gott 1972; Abadi et al. 1999). In contrast, if only the hot gas in the outer parts of galaxies is stripped, the galaxy may continue forming new stars until all fuel is exhausted. Consequently, this "strangulation" (also called "starvation") results in the gradual decline of the star formation rate (Larson et al. 1980; Balogh et al. 1997). Note, however, that both of these gas-stripping processes will primarily modify the color and SFR of a galaxy without transforming the galaxy morphology (e.g., Weinmann et al. 2006; van den Bosch et al. 2008).[18] Satellite galaxies orbiting within dark matter halos may also be subject to tidal stripping as they experience tidal forces due to the central galaxy, other satellite galaxies, and the potential of the halo itself (e.g., Read et al. 2006). Higher-density environments can also lead to enhanced merger rates, which may also affect quenching (Peng et al. 2010). Recently, McGee et al. (2014) pointed out that the gas outflows that are ubiquitous among star-forming galaxies may also affect the quenching of satellites. According to this scenario, which they refer to as "overconsumption," vigorous star formation in recently accreted satellites may drive outflows that will exhaust the gas supply in the absence of cosmological accretion. These authors also demonstrate that the timescale for satellite quenching due to overconsumption can be much shorter than the time for the gas to be stripped through dynamical processes.

Another clue regarding environmental quenching mechanisms is the observed correlation between the properties of satellites (i.e., specific SFR, colors, and gas fraction) and their more massive central galaxies. The correlation is such that the satellites of quiescent centrals are more likely to be quenched than the satellites of star-forming centrals, even at fixed stellar mass. This phenomenon was originally presented by Weinmann et al. (2006) and is referred to as "galactic conformity." There is growing observational evidence of galactic conformity in both the local universe (Kauffmann et al. 2010, 2013; Phillips et al. 2014, 2015; Knobel et al. 2015) and out to $z \sim 2$, even though the signal is weaker at high redshift (Hartley et al. 2015; Hatfield & Jarvis 2016; Kawinwanichakij et al. 2016). Broadly speaking, the different environmental processes discussed here are expected to act with different strengths and over different timescales as a function of galaxy stellar and halo masses. Therefore, measuring how (stellar) mass and environmental quenching evolve with stellar mass and redshift provides constraints on the quenching processes, particularly at higher redshift ($z \gtrsim 1$), when galaxy-specific SFRs are higher.

In this paper, we primarily focus on how the quenching of galaxies correlates with galaxy stellar mass and environment, and how these evolve with redshift. However, we do not attempt to separate our sample into central or satellite galaxies. Rather, we will denote the environmental density, based on the local overdensity of galaxies compared to the mean, as $(1 + \delta)$. We will make use of the deep near-IR imaging and high

[18] Although this is true in the morphology as traced by stellar mass, for the morphology as traced by light in any passband, even in near-IR, the higher luminosity of young stars will make the star formation disks more prominent and will lead to significant changes in the visual appearance of the morphology as the star formation fades (e.g., Fang et al. 2013). We return to this point about "disk fading" in Section 5.

photometric-redshift accuracy from the FourStar Galaxy Evolution (ZFOURGE) survey, which allow us to compute accurate estimates of the environment for galaxies to fainter magnitudes and with higher completeness than is possible with either ground-based spectroscopy ($K_s < 24$ AB mag; Nanayakkara et al. 2016, for emission-line galaxies) or space-based spectroscopy ($JH_{140} <$ 24 AB mag; Fossati et al. 2017). In contrast, the ZFOURGE data provide precise photometric redshifts for galaxies to $K_s \simeq$ 25.5–26 AB mag, substantially fainter than what is possible with spectroscopy. As a result, the ZFOURGE data allow us to study the environmental impact of quenching for galaxies with low stellar mass out to high redshift ($\log(M/M_{\odot}) \simeq 9.5$ at $z = 2$).

Because we quantify quenching as a function of both stellar mass and local environmental density, throughout this paper we refer to "mass quenching" and "environmental quenching" processes. This does not imply that stellar mass and environmental density directly cause quenching. For instance, black hole mass or central stellar mass density may have a more direct relationship with quenching than stellar mass (Woo et al. 2015; Terrazas et al. 2016), but because these quantities correlate with stellar mass, they will result in a measurable "mass quenching" effect. Similarly, the estimator of environmental density that we use may only be correlated with, rather than directly measure, the aspects of a galaxy's location or environment that actually cause quenching.

The outline of this paper is as follows. In Section 2, we describe the ZFOURGE catalog and our galaxy sample selection criteria. In Section 3, we describe the method for estimating the environmental densities using photometric redshifts, and we validate our method using simulated catalogs from a semi-analytic model (described further in Appendix A). In Section 4, we discuss how the fraction of quiescent galaxies varies with stellar mass and environment, and we compute from these the quenching efficiency for both variables out to $z = 2$. In Section 5, we discuss the relative importance of environmental processes in the build-up of red galaxies in dense environments. We investigate whether the cause of environmental quenching is indicated in the morphological distribution of lower-mass quiescent galaxies. In addition, we consider how our results constrain the timescales of environmental quenching and therefore the physical processes responsible. In Section 6, we present our summary. Throughout, we adopt the following cosmological parameters where appropriate: $H_0 = 70$ km s^{-1} Mpc^{-1}, $\Omega_m = 0.3$, and $\Omega_{\Lambda} = 0.7$. All magnitudes are expressed in the AB system.

2. Data and Sample Selection

We select galaxies at $0.5 < z < 2.0$ from the ZFOURGE survey (Straatman et al. 2016). The survey is composed of three $11' \times 11'$ fields with coverage in the regions of CDFS (Giacconi et al. 2002), COSMOS (Scoville et al. 2007), and UDS (Lawrence et al. 2007) that overlap with the Cosmic Assembly Near-IR Deep Extragalactic Legacy Survey (CANDELS; Grogin et al. 2011; Koekemoer et al. 2011), which also provide *Hubble Space Telescope* (*HST*), high-angular resolution imaging for 0.6–1.6 μm (see, e.g., van der Wel et al. 2012). The ZFOURGE medium-band near-IR imaging reaches depths of ~26 AB mag in J_1, J_2, J_3 and ~25 AB mag in H_s, H_l and includes the vast amount of deep, multiwavelength imaging available in these legacy fields. The ZFOURGE catalogs are complete for galaxies to $K_s \simeq 25.5 - 26.0$ AB mag (see Straatman et al. 2016).

2.1. Photometric Redshifts

The ZFOURGE catalogs include photometric redshifts and rest-frame colors calculated using EAZY (Brammer et al. 2008) from the 0.3 to 8 μm photometry for each galaxy. Of import here is that ZFOURGE uses templates and photometric zeropoints that are iteratively adjusted during the fitting process to improve the accuracy of the photometric redshifts.

The precision of photometric redshifts has the ability to potentially introduce spurious signals or wash out structure (Cooper et al. 2005; Quadri et al. 2012). However, our estimates of the quality of the ZFOURGE photometric redshifts show them to be very accurate, and as we demonstrate below, sufficient to recover galaxy environmental densities. By comparing photometric redshifts of galaxy pairs and to spectroscopic subsamples, Straatman et al. (2016) show that the typical photometric-redshift uncertainties are $\sigma_z/(1+z) = 0.01$–0.02 to the K_s-band magnitude limit for galaxies between $z = 0.5$ and $z = 2.0$, with negligible dependence on galaxy color, but there is dependence on magnitude and redshift (Straatman et al. 2016, see their Section 5.4). Quantitatively, at $K_s < 25.0$ AB mag, the photometric-redshift uncertainties of quiescent galaxies at $z = 2$ are better than those of star-forming galaxies at the same redshift —only about 5%. Other studies with ZFOURGE have shown that these redshifts are sufficient to identify protoclusters out to $z \sim 2$ (e.g., Spitler et al. 2012; Yuan et al. 2014; Forrest et al. 2017).

In addition to the photometric redshifts, we also make use of stellar masses for galaxies provided in the ZFOURGE catalogs. The stellar masses were derived by fitting stellar population models to the photometry using FAST (Kriek et al. 2009), assuming exponentially declining star formation histories, solar metallicity, and a Chabrier (2003) initial mass function.

2.2. Stellar Mass Completeness

Because we are concerned with the galaxy quiescent fractions, it is important that we use a data set that is complete in stellar mass for both star-forming and quiescent galaxies. Quiescent galaxies have higher mass-to-light ratios and therefore will have a higher mass-completeness limit than star-forming galaxies at fixed magnitude. Here, we adopt 90% mass-completeness limits for galaxies with a quiescent stellar population using the technique described by Quadri et al. (2012). In a given narrow redshift bin, we select all quiescent galaxies and scale their fluxes (and therefore their stellar masses) downward until they have the same magnitude as the measured magnitude limit, $K_s = 25.5$ AB mag, for all three ZFOURGE fields. Then, we define the mass-completeness limit as the stellar mass at which we recover 90% of the dimmed galaxies at each redshift. We provide the adopted completeness limits for ZFOURGE at $0.5 < z < 2.5$ in Table 1.

2.3. Selection of Quiescent and Star-forming Galaxies

Our goal is to measure the fraction of quiescent galaxies as a function of stellar mass, environment, and redshift. From the parent sample of all galaxies in the ZFOURGE catalog, we first select all well-detected galaxies (USE flag = 1) and group them into three bins of redshift, $0.5 < z < 1.0$, $1.0 < z < 1.5$, and $1.5 < z < 2.0$. We then further subdivide the samples into bins of galaxy stellar mass, $8.8 < \log(M/M_{\odot}) < 9.8$, $9.8 < \log(M/M_{\odot}) < 10.5$, and $10.5 < \log(M/M_{\odot}) < 11.5$. In each of these bins, we classify galaxies as either star

Table 1
Stellar Mass-completeness Limits for ZFOURGE Galaxies at $0.5 < z < 2.5$

Redshift	$\log(M/M_{\odot})$	Redshift	$\log(M/M_{\odot})$
0.5	8.09	1.6	9.24
0.6	8.25	1.7	9.31
0.7	8.40	1.8	9.38
0.8	8.52	1.9	9.44
0.9	8.64	2.0	9.51
1.0	8.74	2.1	9.57
1.1	8.84	2.2	9.62
1.2	8.93	2.3	9.68
1.3	9.01	2.4	9.73
1.4	9.09	2.5	9.79
1.5	9.17	...	...

forming or quiescent using their rest-frame $U-V$ and $V-J$ colors, denoted by $(U-V)_0$ and $(V-J)_0$, respectively. This *UVJ* color–color space is useful to separate galaxies with colors of quiescent and star-forming stellar populations (including the effects of dust attenuation; Williams et al. 2009; Patel et al. 2012). Due to the small systematic variations in the rest-frame colors of galaxies at fixed stellar mass and redshift in different surveys, we follow our previous method (Kawinwanichakij et al. 2016, see Section 2.2 in that paper) to self-calibrate the region in the *UVJ* color–color space to delineate star-forming from quiescent galaxies. We then select quiescent galaxies whose rest-frame colors satisfy

$$\begin{aligned}(U-V)_0 &> 1.2 \times (V-J)_0 + 0.2\\ (U-V)_0 &> 1.3\\ (V-J)_0 &< 1.6.\end{aligned} \quad (1)$$

A summary of the number of galaxies from each galaxy mass, redshift, and density subsample is given in Table 2.

Figure 1 shows the *UVJ* color–color diagram for galaxies in our ZFOURGE samples at $0.5 < z < 2.0$ split into low stellar mass $(8.8 < \log(M/M_{\odot}) < 10.2)$ and high stellar mass $(10.2 < \log(M/M_{\odot}) < 11.5)$ subsamples, and as a function of environment as defined by local overdensity (see Section 3 below). Although all panels show a similar range of galaxy colors, differences in the distributions are clearly evident with mass (and also environment). The distribution of lower-mass galaxies is weighted more toward bluer star-forming objects (by number), while the distribution of higher-mass star-forming galaxies show higher dust attenuation, consistent with other studies (e.g., Wuyts et al. 2011). All panels also show the existence of a "red sequence" of quiescent galaxies, but this is much more pronounced in the higher-density regions (denser environments), which we discuss more below.

2.4. Structural Morphological Parameters

In our analysis, we study the morphological differences between quiescent and star-forming galaxies in different environments and as a function of stellar mass. The majority of galaxies in our sample fall within the CANDELS coverage from *HST*/WFC3, with the effective semimajor axis, $a_{\rm eff}$, and Sérsic index, n, measured by van der Wel et al. (2012) using the *HST*/WFC3 F160W (H_{160})-band imaging. We refer the reader to van der Wel et al. for the measurement of the random and systematic uncertainties of the estimated morphological parameters using simulated galaxy images. We cross-matched the sources in our catalog with those of van der Wel et al. The fractions of our galaxy sample with available morphological parameters from van der Wel et al. are 80%, 90%, and 82% for CDFS, COSMOS, UDS, respectively. We note that 10%–20% of our galaxy sample have no morphological information from *HST*/WFC3 because those galaxies are in the regions around the edges of ZFOURGE fields where there is no *HST*/WFC3 coverage. We further define the circularized effective radius as $r_{\rm eff} = a_{\rm eff}\sqrt{q}$, where $a_{\rm eff}$ is the effective semimajor axis and $q = b/a$ is the ratio of the semiminor to semimajor axis. In addition to the morphological parameters from van der Wel et al., we calculate the inner 1 kpc of the stellar mass surface density, the procedure for which we describe in Appendix B.

3. Measurement of Galaxy Density as an Estimate of Environment

In this work, we estimate the local galaxy (projected) overdensity using the distance to the Nth nearest neighbor, d_N. This distance has often been used as a measure of the overdensity, with N typically varying from 3 to 10 (e.g., Dressler 1980; Baldry et al. 2006; Muldrew et al. 2012). We are then able to define the environment of a galaxy in terms of the dimensionless overdensity, $1+\delta$, defined as

$$(1+\delta)_N = 1 + \frac{\Sigma_N - \langle\Sigma\rangle}{\langle\Sigma\rangle}, \quad (2)$$

where $\Sigma_N = N/(\pi d_N^2)$ is the local surface density of a galaxy based on the distance to the Nth nearest neighbor and $\langle\Sigma\rangle$ is the average surface number density of galaxies over the whole field. We then take $(1+\delta)$ to denote the fractional density of galaxies with respect to the mean (as a function of redshift).

We improve our measurement of overdensity using an estimator for the Nth nearest neighbor introduced by Ivezić et al. (2005). The distances to all N nearest neighbors provide the information about the local density (overdensity) of galaxies. Motivated by the Bayesian probability framework, we incorporate the projected distance to the Nth nearest neighbors into the density estimator, and we additionally take into account information from the projected distances to the first $N-1$ nearest neighbors. Ivezić et al. demonstrate that this increases the accuracy of the overdensity compared to the traditional Nth nearest neighbor metric because it uses the distances to the first, second, ... Nth neighbors and is less subject to projection effects (see Appendix B of Ivezić et al. 2005). One of the advantages of this estimator is that it provides a good estimate of the "local density," which corresponds to scales internal to galaxy group halos, provided N is relatively small (see Muldrew et al. 2012). As many of the environmental trends we find appear to correlate with group-sized halos, we adopt $N = 3$ for the analysis here. Specifically, we use the estimator as given by Cowan & Ivezić (2008):

$$\Sigma'_N = C\frac{1}{\Sigma_{i=1}^{N} d_i^2}. \quad (3)$$

Here, we take the third nearest neighbor (3NN) distance, where we empirically determine the constant, C, by requiring that $\langle\Sigma'_N\rangle$ be equal to that for a uniform density of galaxies with the same total number and area as in our ZFOURGE data set.

Table 2
Number of Quiescent and Star-forming Galaxies in Different Stellar Mass and Density Quartiles in ZFOURGE at $0.5 < z < 2.0$

Stellar Mass Range	Redshift Range	Lowest-density Quartile			Highest-density Quartile		
		$N_{\rm Quiescent}$	$N_{\rm Star\text{-}forming}$	$N_{\rm Total}$	$N_{\rm Quiescent}$	$N_{\rm Star\text{-}forming}$	$N_{\rm Total}$
$8.8 < \log(M/M_{\odot}) < 9.8$	$0.5 < z < 1.0$	24	662	686	113	427	540
	$1.0 < z < 1.5$	10	491	501	22	406	428
	$1.5 < z < 2.0$	8	259	267	5	212	217
$9.8 < \log(M/M_{\odot}) < 10.5$	$0.5 < z < 1.0$	39	129	168	96	138	234
	$1.0 < z < 1.5$	32	146	178	42	144	186
	$1.5 < z < 2.0$	24	196	220	40	165	205
$10.5 < \log(M/M_{\odot}) < 11.5$	$0.5 < z < 1.0$	30	33	63	87	50	137
	$1.0 < z < 1.5$	15	37	52	51	51	102
	$1.5 < z < 2.0$	19	64	83	54	74	128

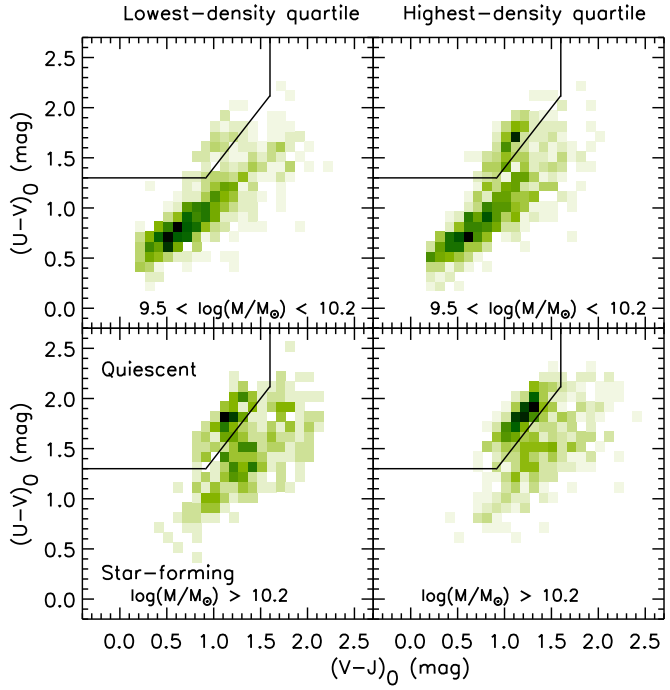

Figure 1. Rest-frame $U - V$ vs. rest-frame $V - J$ color for galaxies at $0.5 < z < 2.0$ in the lowest-density quartile (left panels) and the highest-density quartile (right panels), with lower stellar masses $9.5 < \log(M/M_{\odot}) < 10.2$ (top panels) and higher stellar masses $\log(M/M_{\odot}) > 10.2$ (bottom panels). In each panel, the darkness of the shading is proportional to the number of galaxies in that region. Galaxies in the upper-left region of each plot (separated by the solid line) have colors of quiescent stellar populations; galaxies outside this region have colors of star-forming populations combined with dust attenuation (see Williams et al. 2009).

For this study, we calculate the 3NN distance, Σ'_3, for each galaxy in the ZFOURGE catalog. At each redshift, we consider all galaxies more massive than the mass-completeness limits given in Table 1. For each galaxy, we measure the density only considering galaxies with a photometric-redshift separation that is 2.5 times the estimated redshift uncertainty, i.e., $2.5 \times 0.02(1 + z_{\rm phot})$, where we adopt the factor of 0.02 as a conservative redshift uncertainty. We then compute the overdensity of galaxies, $\log(1 + \delta')_3$, using the Bayesian-motivated estimate of the local surface density of galaxies derived from the third nearest neighbor by substituting Σ'_3 into Σ_N of Equation (2). In Appendix A, we verify using a mock galaxy catalog that this method recovers well the true projected overdensity for data with the photometric accuracy of ZFOURGE in that it faithfully recovers galaxies in the highest and lowest density quartiles with a minimal amount of contamination. Our tests also showed that $N = 3$ provides a good compromise between the accuracy of the measured galaxy overdensity and the ability to probe group-sized environments, which is appropriate for our study here. However, we experimented using Σ'_N with $N = 2$, 5, and 7 and find that our main conclusions are unaffected by the choice of N.

In addition, we tested for "edge effects" by excluding galaxies from our analysis that are ∼20 arcsec (larger than the 3NN distances for the galaxies in the lowest-density quartile) from the survey edges. This does not affect the main results for the differences in the quiescent fractions as a function of stellar mass and environment that are presented in Section 4. To be even more conservative, we then tested for edge effects by excluding galaxies that are twice that distance from the survey edges (∼40 arcsec), and find no change in our results, although the uncertainties in the quiescent fractions increase as the sample size decreases. We therefore apply no correction for the edge effects in this study.

Figure 2 shows the projected density, Σ'_3, and overdensity, $\log(1 + \delta')$, computed from the 3NN (Σ'_3) of each ZFOURGE galaxy as a function of redshift. We calculated the median, bottom, and top quartiles of the distribution (i.e., the bottom and top 25th percentiles) to determine the relative overdensity of each galaxy. We determined these quartiles using a spline linear regression implemented with the COnstrained B-Splines (cobs) package in R (Ng & Maechler 2007; Feigelson & Babu 2012). We find that, over the redshift range 0.5–2.0, the projected density (Σ'_3) at the lower and upper quartiles of overdensity are about 13 and 43 galaxies per arcmin^2, respectively. In the following analysis, we define a galaxy to be in a low (high)-density environment if it has an overdensity $\log(1 + \delta')$ less (greater) than the lower (upper) 25th percentile. We will interchangeably use the terms low/high-density environments (hereafter δ_{25}/δ_{75}) with the lowest-/highest-density quartiles.

4. Results

In this section, we calculate the quiescent fraction as a function of stellar mass and environment, using the

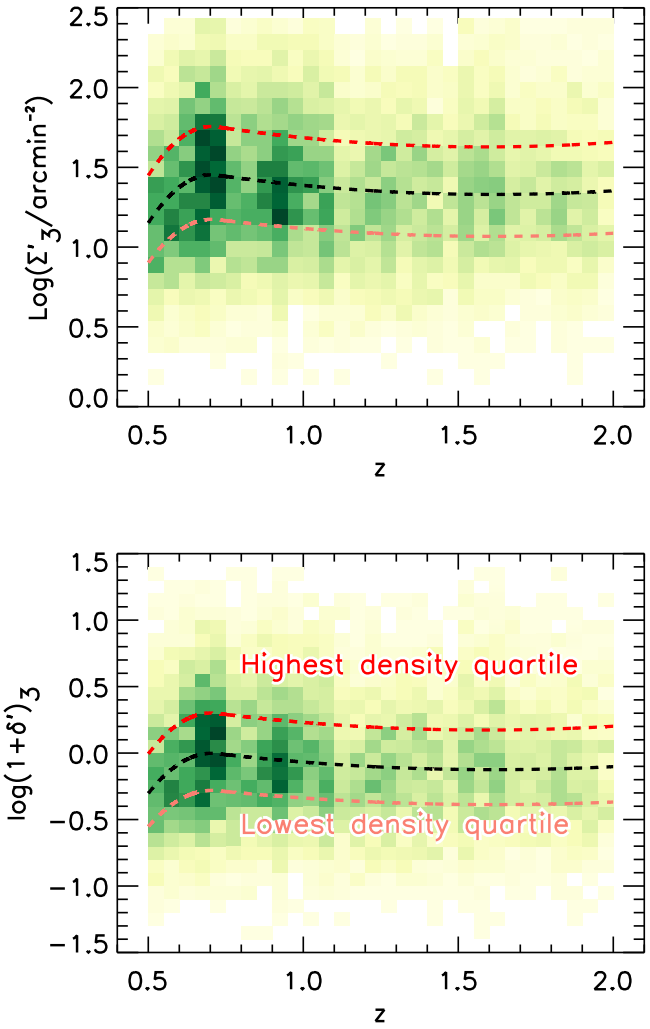

Figure 2. Top: projected density computed from the Bayesian third nearest neighbor (Σ_3') of each galaxy in three combined ZFOURGE fields as a function of redshift. The black, light-red, and red dashed lines show the median, bottom, and top quartiles (25th percentiles) of the distribution, derived from a spline quartile regression applied to the data (see text). Bottom: corresponding overdensity of ZFOURGE galaxies as a function of redshift computed using the same method. We again show the median, bottom, and top quartiles. We define galaxies in the upper and lower quartiles of overdensity to be in "high-" and "low-"density environments, respectively. In each panel, the darkness of the shading is proportional to the number of galaxies in that region.

overdensities ($1 + \delta'$) derived above. We use these fractions to estimate the environmental quenching efficiency and (stellar) mass quenching efficiency as defined below.

4.1. Evolution of Quiescent Fraction with Environment and Redshift

We show the quiescent fraction of galaxies as a function of the overdensity in Figure 3. We apply a mass limit of $\log(M/M_\odot) > 9.5$ in all three redshift bins, which corresponds to our completeness limit at $z = 2.0$. We also compare our quiescent fraction with those from Quadri et al. (2012), who used the galaxy sample from the UKIDSS Ultra-Deep Survey, so we apply a mass limit of $\log(M/M_\odot) > 10.2$, corresponding to the completeness limit at $z = 2.0$ used by Quadri et al. (2012). The error bars indicate the 1σ uncertainty based on Poisson statistics for the number of quiescent galaxies in a bin. At all redshift ranges, we see evidence for a higher quiescent fraction of galaxies at higher densities. This effect is very strong at $z < 1$ (left panel of Figure 3), but decreases at higher redshift, $z > 1$ (middle and right panels of Figure 3). This is in agreement with previous studies of the star formation–density relation (e.g., Quadri et al. 2012), where with the ZFOURGE data we have extended the result to lower masses and higher redshifts (for a recent study of a galaxy sample with stellar mass and redshift range comparable to our sample, see Guo et al. 2017).

In this section, we showed that the quiescent fraction of galaxies is higher in denser environments over all redshifts probed in this study. In principle, it is possible that this result is caused by differences in the stellar mass distribution and/or the redshift distribution of quiescent and star-forming galaxies. To check for this, we create samples of quiescent and star-forming galaxies such that their stellar mass and redshift distributions are matched following the method described by Kawinwanichakij et al. (2016, see their Section 3.2). The left panel of Figure 4 shows the differences in overdensity between the quiescent and star-forming galaxies before this matching at $1.5 < z < 2.0$ (a p-value of the differences as measured by a K–S test of $\ll 10^{-3}$), and the right panel shows that the difference persists even after matching the stellar mass and redshift distributions (a p-value of $\ll 10^{-3}$). We obtain even more significant results in our other (lower) redshift bins. We conclude that, at all redshifts studied here, quiescent galaxies are more common in overdense regions compared to star-forming galaxies even taking into account differences in redshift and stellar mass.

4.2. Evolution of Quiescent Fraction with Stellar Mass and Redshift

Figure 5 shows the quiescent fraction as a function of stellar mass in bins of redshift, separating galaxies in the highest (δ_{75}) and lowest (δ_{25}) density quartiles. Qualitatively, at $0.5 < z < 1.5$, galaxies in the highest-density quartile show higher quiescent fractions than galaxies with the same mass in the lowest-density quartile in all stellar mass bins. This is in agreement with Allen et al. (2016), who show that the fraction of quiescent galaxies with $\log(M/M_\odot) \gtrsim 9.5$ at $z \sim 0.95$ increases with decreasing distance to the cluster core. At higher redshift, $1.5 < z < 2.0$, this trend persists for more massive galaxies ($\log(M/M_\odot) \gtrsim 10$).

Figure 6 shows the quiescent fraction as a function of redshift in bins of stellar mass, separating out the lowest and highest-density quartiles. Qualitatively, galaxies have higher quiescent fractions in high-density environments compared to galaxies in low-density environments out to $z \sim 2$ and for galaxies with stellar mass $\log(M/M_\odot) \gtrsim 9.8$. For lower stellar mass galaxies ($8.8 < \log(M/M_\odot) < 9.8$), the quiescent fractions are higher in the higher-density environment at least to $z \lesssim 1.5$, but at higher redshift, $z \gtrsim 1.5$, the quiescent fraction shows less dependence on environment.

The range of quiescent fraction as a function of overdensity and stellar mass is large, ranging from nearly 100% to less than 1%. To illustrate this, we show the quiescent fraction in log scale instead of linear scale in both Figures 5 and 6. This better presents the separation of quiescent fractions of galaxies in different environments and also the relative quiescent fraction in each stellar mass bin. Because more massive galaxies tend to exist in higher-density environments, it is logical to ask to what extent this drives the trend among mass, redshift, and environment. This is a reasonable question, as the number

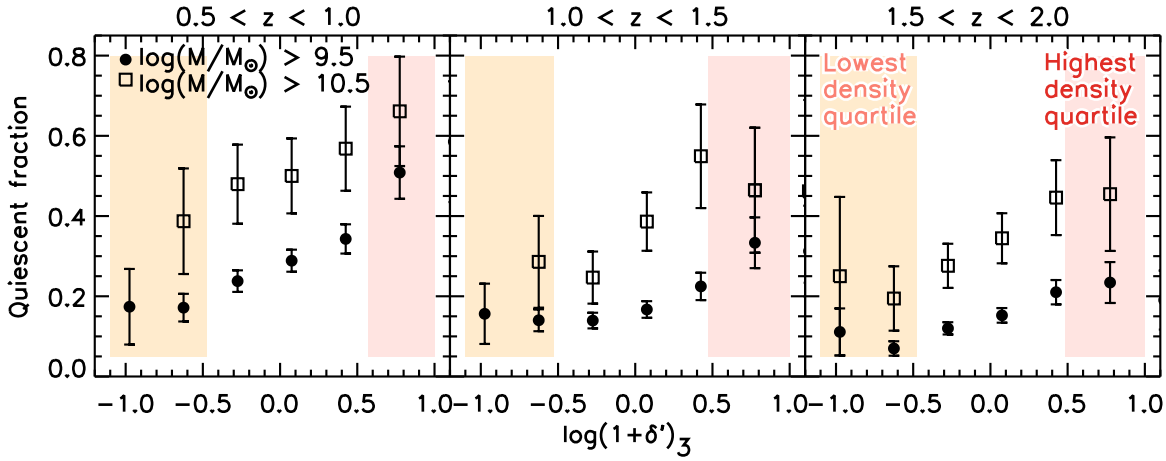

Figure 3. Quiescent fraction vs. overdensity in three different redshift ranges for two mass-selected samples. The quiescent fractions of galaxies are determined in bins of 0.4 dex of $\log(1+\delta')$. The error bars indicate 1σ uncertainties based on Poisson statistics. The shaded regions in each panel indicate the lower and upper 25th percentiles of $\log(1+\delta')$, where we define low- and high-density environments.

density of quiescent galaxies, even at high redshift, increases with both stellar mass and environment (e.g., C. Papovich et al. 2017, in preparation).

To answer this, we perform a similar procedure to Quadri et al. (2012). We computed the mean overdensity of quiescent and star-forming galaxies in narrow 0.25 dex bins in stellar mass (where we expect such narrow bins to have a negligible change in overdensity), which we show in Figure 7. This figure shows evidence that quiescent galaxies have a higher overdensity than mass-matched star-forming galaxies (down to the stellar mass limit of each redshift), and this trend exists to $z \sim 2$. These trends extend correlations found by Quadri et al. (2012) to lower stellar masses. In particular, the density contrast between star-forming and quiescent galaxies is largest for lower-mass galaxies, $\log(M/M_{\odot}) \simeq 9$–10. As argued by Quadri et al. (2012), this suggests that the environment plays a dominant role in galaxy quenching, and here we show this extends to the lowest stellar masses. Our analysis supports this assertion, which we discuss more below.

4.3. Environmental and Stellar Mass Quenching Efficiencies

To quantify the environment and stellar mass in quenching the star formation activity in galaxies, we follow the approach of Peng et al. (2010, which is similar to the methods of van den Bosch et al. 2008; Quadri et al. 2012; Kovač et al. 2014; Lin et al. 2014). We define the environmental quenching efficiency, $\varepsilon_{\rm env}$, as the fraction of galaxies at a given stellar mass, M, that are quenched in excess of those in the lowest-density environment (presumably these are galaxies that would be forming stars in the lowest-density environments, but have had their star formation truncated due to some physical process related to the environment). The environmental quenching efficiency is then

$$\varepsilon_{\rm env}(\delta,\, \delta_0,\, M) = \frac{f_q(\delta,\, M) - f_q(\delta_0,\, M)}{1 - f_q(\delta_0,\, M)}, \tag{4}$$

where f_q is the quiescent fraction for galaxies with stellar mass M and overdensity, δ. δ_0 is the overdensity of the low-density reference environment, where we choose $\delta_0 = \delta_{25}$, i.e., the overdensity demarcating the lowest 25th percentile of the overdensity distribution (see Figure 2). We note, however, that we are parameterizing non-environmental quenching with stellar mass because it correlates with the other quantities associated with (stellar) mass quenching such as the central stellar mass and black hole mass (e.g., Woo et al. 2013, 2015, 2017b; Zolotov et al. 2015; Tacchella et al. 2016a, 2016b; Terrazas et al. 2016)

For galaxies with $\delta \leqslant \delta_{25}$, our definition of $\varepsilon_{\rm env}$ explicitly assumes that environment quenching is negligible (i.e., $\varepsilon_{\rm env}(\delta < \delta_0) \approx 0$) for all stellar masses. This is a reasonable assumption as there is no apparent evolution in the shape of the quiescent galaxy stellar mass function in low-density environments over the redshift and stellar mass range considered here (C. Papovich et al. 2017, in preparation), as would be expected if galaxy quenching correlates only with stellar mass. For the remainder of this paper, we will also denote the (stellar mass-dependent) quiescent fraction of galaxies in the lowest- and highest-density quartiles as $f_q(\delta_{25}, M)$ and $f_q(\delta_{75}, M)$, respectively.

Similarly, we define the (stellar) mass quenching efficiency $\varepsilon_{\rm mass}$ as the fraction of galaxies at a fixed overdensity, $\log(1+\delta)$, that are quenched compared to the star-forming fraction at low masses. Specifically, we define the mass quenching efficiency to be,

$$\varepsilon_{\rm mass}(M,\, M_0,\, \delta) = \frac{f_q(\delta,\, M) - f_q(\delta,\, M_0)}{1 - f_q(\delta,\, M_0)}, \tag{5}$$

where in practice we take the reference mass M_0 to be the stellar mass at the completeness limit for a given redshift, and we compute the mass quenching efficiency for galaxies with $\delta < \delta_{75}$.

4.4. Dependence of Quenching Efficiencies on Stellar Mass and Redshift

Figure 8 compares the strength of the environmental quenching and (stellar) mass quenching efficiencies as a function of stellar mass for galaxies in the highest-density environments ($\delta \geqslant \delta_{75}$). At all redshifts, the (stellar) mass quenching efficiency increases with stellar mass. At $1 < z < 1.5$ and $1.5 < z < 2$, the magnitude of environmental quenching efficiency is on par with the (stellar) mass quenching

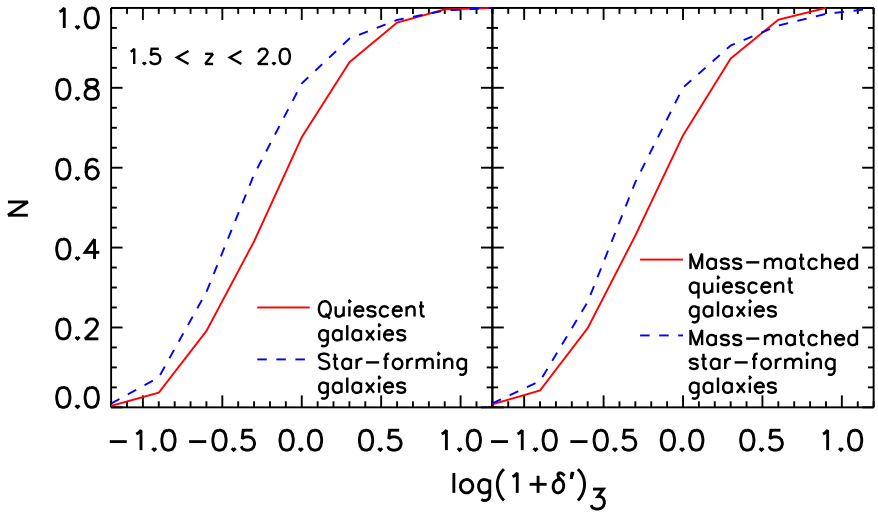

Figure 4. Left: cumulative distribution of overdensities $\log(1+\delta')$ for quiescent galaxies (red solid line) and star-forming galaxies (blue dash lines) with $\log(M/M_{\odot}) > 9.5$ at $1.5 < z < 2.0$. A K–S test indicates that we can reject the null hypothesis that these two distributions are drawn from the same parent distribution with a p-value of $\ll 10^{-3}$ Right: same as the left panel but for mass-matched and redshift-matched samples of quiescent and star-forming galaxies. A K–S test indicates that the differences in the distributions persists with a p-value of $\ll 10^{-3}$.

efficiency: in the highest-density environments, roughly half of all galaxies are quenched by the environment.

At lower redshifts, $0.5 < z < 1$, the evolution of the environmental quenching efficiency is strongest for lower-mass galaxies. For example, in the mass range $8.8 < \log(M/M_{\odot}) < 10$, $\varepsilon_{\rm env}$ increases from $<10\%$ at $z > 1$ to $\sim 30\%$ at $z < 1$. Moreover, at these redshifts, the environmental quenching efficiency dominates over (stellar) mass quenching efficiency for these lower-mass galaxies (in the highest-density environments). Therefore, in the highest-density environments, the majority of quiescent lower-mass galaxies have been quenched by environmental processes rather than by other processes (see also Hogg et al. 2003; van den Bosch et al. 2008; Quadri et al. 2012). Comparing the magnitudes of the environmental and (stellar) mass quenching efficiencies gives an estimate of the effect, which is of order $\varepsilon_{\rm env}/\varepsilon_{\rm mass} > 5$ for galaxies with $\log(M/M_{\odot}) =$ 8.8–9.8, i.e., the environment accounts for the quenching of five out of six galaxies in this mass range.

Figure 8 also shows that at $0.5 < z < 1.0$, the environmental quenching efficiency appears to be nearly independent of stellar mass. At $z > 1$, the environmental quenching efficiency shows a clearer dependence on stellar mass: more massive galaxies experience stronger environmental quenching. This persists at least to $z \simeq 2$ for galaxies with $\log(M/M_{\odot}) > 9.8$.

We explore the evolution with redshift of both the environmental quenching efficiency and the mass quenching efficiency for galaxies in three stellar mass bins: $9.5 < \log(M/M_{\odot}) < 9.8$, $9.8 < \log(M/M_{\odot}) < 10.2$, and $\log(M/M_{\odot}) > 10.2$ in Figure 9. At lower redshifts, $0.5 < z < 1$, the environmental quenching efficiency of galaxies at all masses is ≈ 0.3. This is generally consistent with that measured with the same (relatively higher) stellar mass at $0.3 < z < 0.6$ from zCOSMOS (Peng et al. 2010). However, this "constant" quenching efficiency is a coincidence of epoch. At higher redshifts, the environmental quenching efficiency of low-mass galaxies decreases and is very low ($\lesssim 5\%$) at $z > 1.5$, while for more massive galaxies it remains roughly constant (or possibly slightly declining) out to $z \sim 2$. The evolution of the environmental quenching efficiency depends both on redshift and stellar mass, and its effects are not separable from stellar mass at higher redshift.

Comparing to the literature, the environmental quenching efficiency we derive at $1 < z < 1.5$ is modestly lower than that derived for a sample of spectroscopically confirmed galaxy clusters at $0.87 < z < 1.63$ with $\log(M/M_{\odot}) > 10.3$ from the *Spitzer* Adaptation of the Red-Sequence Cluster Survey (SpARCS; Nantais et al. 2016). However, this may be expected as the SpARCS sample includes very rich clusters at these redshifts, which include galaxies in even higher overdensities than the galaxies in our highest-density environments in ZFOURGE. Our result of increasing quiescent fractions in high-density environments implies that the strength of the environment quenching efficiency increases with overdensity, and it is very reasonable that this efficiency is even higher in the rich environments of galaxy clusters.

Figure 9 also shows that the strength of the (stellar) mass quenching efficiency increases with increasing stellar mass and decreasing redshift. This is consistent with the overall decrease in star formation activity in galaxies at later cosmic times (e.g., Madau & Dickinson 2014).

5. Discussion

5.1. On the Environmental Impact on Quenching

Our main result is that there is strong evidence for both (stellar) mass quenching and environmental quenching for galaxies to high redshift. For massive galaxies, $\log(M/M_{\odot}) > 10.2$, environmental quenching is evident, and nearly unchanging (or slowly declining), over the redshift range of our sample, $0.5 < z < 2$. For lower-mass galaxies, the environmental quenching efficiency evolves strongly with redshift, at least to $\log(M/M_{\odot}) = 9.5$, where our data are complete. For such lower-mass galaxies, the environmental quenching declines by roughly an order of magnitude from $z = 0.5$ to 2. At our lower redshift range, $0.5 < z < 1.0$, the environmental quenching efficiency dominates over the (stellar) mass quenching efficiency by a factor of >5:1 for galaxies with $\log(M/M_{\odot}) = 8.8$–9.8 (Figure 8). Therefore, the majority of low-mass quiescent galaxies are quenched by their environment (Hogg et al. 2003;

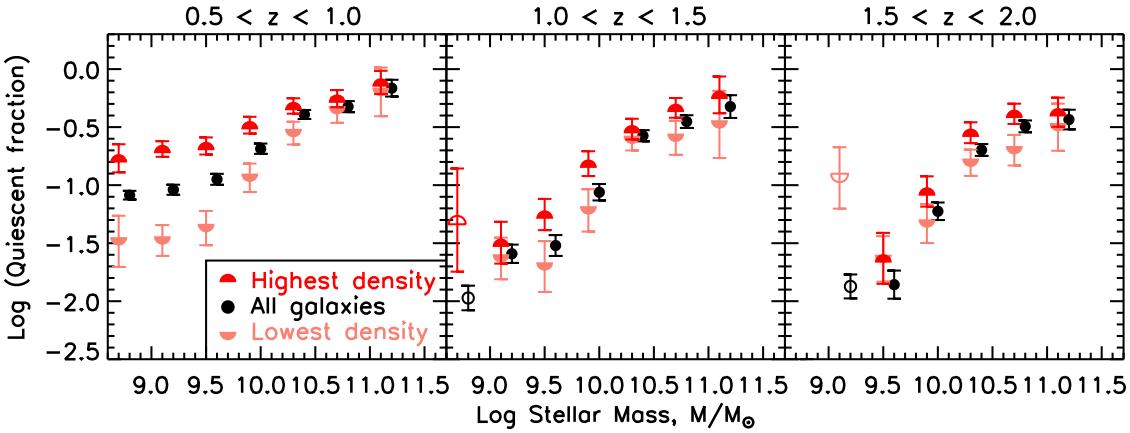

Figure 5. Quiescent fraction vs. stellar mass in three different redshift ranges for all galaxies (black circles), galaxies in the highest-density quartile (red upper-half circles), and galaxies in the lowest-density quartile (light-red lower-half circles). The quiescent fractions are determined in bins of 0.4 dex in $\log(M/M_{\odot})$. Open symbols correspond to data below each subsample's respective mass-completeness limit. The error bars indicate 1σ uncertainties based on Poisson statistics. The quiescent fractions of all galaxies (black circles) are slightly offset along the abscissa for clarity. Galaxies in denser environments have a higher quiescent fraction in all stellar mass bins out to $z \sim 2.0$, except possibly for the lowest-mass galaxies ($\log(M/M_{\odot}) \simeq 9$–10) at $1.5 < z < 2.0$.

Quadri et al. 2012). Our result here is consistent with that of Geha et al. (2012), who found that the number of quiescent low-mass galaxies with $7 < \log(M/M_{\odot}) < 9$ in the field is very low (<0.06%), demonstrating that star formation in low-mass galaxies ($\log(M/M_{\odot}) < 9$) are suppressed by being near more massive galaxies (although see Geha et al. 2017). In addition, our results are in excellent agreement with the recent study by Guo et al. (2017), who used CANDELS data to measure the distance from low-mass galaxies to the nearest massive neighbor galaxies. They found that environmental quenching is the dominant quenching mechanism for galaxies with $\log(M/M_{\odot}) <$ 9.5 out to $z \sim 1$. At higher redshift, Guo et al. (2017) observed minimal environmental quenching for low-mass galaxies, which is consistent with our finding here, but our observation with the ZFOURGE survey provides us with sufficient statistics and accurate environment measurements (due to the precise photometric redshifts) to strengthen this result.

We note that at $0.5 < z < 1.0$, even in low-density environments, the fraction of massive quiescent galaxies with stellar mass $\log(M/M_{\odot}) \gtrsim 10.8$ is comparable to those in the high-density environment. The observation of quiescent galaxies in voids (low-density environment) has been reported by Croton et al. (2005). Croton & Farrar (2008) further compared the luminosity function of void galaxies in the 2dF Galaxy Redshift Survey to that from a galaxy formation model built on the Millennium simulation. These authors demonstrated that a population of quiescent galaxies in low-density environments will arise naturally due to a combination of a shift in the halo mass function in low-density environments and an environment independent of a star formation suppression mechanism efficient above a critical halo mass of $M_{\rm vir} \sim 10^{12.5} M_{\odot}$ (radio-mode AGN).

Some hint of the quenching mechanism comes from the timescales and the evolution in the quenching efficiency. The lack of significant environmental quenching in low-mass galaxies at $z > 1$ suggests that the quenching timescale is at least 3–5 Gyr (corresponding to the lookback time from $z = 1$ to an infall epoch of $z = 3$–6). This is consistent with quenching times from other studies of environmental processes (e.g., Peng et al. 2010, 2015; Tinker & Wetzel 2010; Quadri et al. 2012; Slater & Bell 2014; Wetzel et al. 2015; Darvish et al. 2016; Fossati et al. 2017; Guo et al. 2017). Several recent studies (e.g., Fillingham et al. 2015; Peng et al. 2015; Davies et al. 2016) argue that environmental quenching for galaxies with $\log(M/M_{\odot}) = 8.0$–10.0 are primarily driven by starvation because quenching timescales and cold gas-depletion timescales are comparable. For more massive galaxies, $\log(M/M_{\odot}) \gtrsim 10$, the quenching timescale could be shorter, given that we see higher environmental quenching efficiency for these galaxies even in our highest redshift bin, $1.5 < z < 2.5$. This suggests a mass-dependent quenching mechanism, such as "over-consumption" (McGee et al. 2014), which arises as more massive (star-forming) galaxies have shorter gas-depletion times (which we discuss more below). Our results support these findings, but with the additional requirement (also discussed below) that the quenching process also transform the morphologies of the quenching galaxies.

The environmental processes driving the quenching must occur in environments with overdensities comparable to those of our high-density quartile. The ZFOURGE fields contain some massive groups (Fossati et al. 2017) but no massive, virialized clusters given the cosmological volume contained in the ZFOURGE/CANDELS fields. Furthermore, our overdensity estimator based on the third nearest neighbor distance measurements are primarily sensitive to group-sized scales (Muldrew et al. 2012). Therefore, the environmental quenching efficiency we measure pertains to physical mechanisms within such environments and not necessarily to more massive clusters, which may have even stronger environmental quenching efficiency. In addition, even though we do not separate our galaxy sample into central and satellite galaxies in this study, we note that if environmental effects are specific to satellite galaxies, the observed trend here would be even stronger (see Fossati et al. 2017).

5.2. On the Lack of Environmental Impact on Morphology

One way to constrain the cause or causes of environmental quenching is to test if they also affect the morphological structures of the quenched galaxies. Previous studies have demonstrated a relation between galaxy morphology and star formation activity, quenched fractions, and implied gas fractions (e.g., Franx et al. 2008; Wuyts et al. 2011; Bell et al. 2012; Papovich et al. 2015), and quenching is driven by the processes that change morphology and grow black holes (non-environmental effects which we refer to as "(stellar) mass

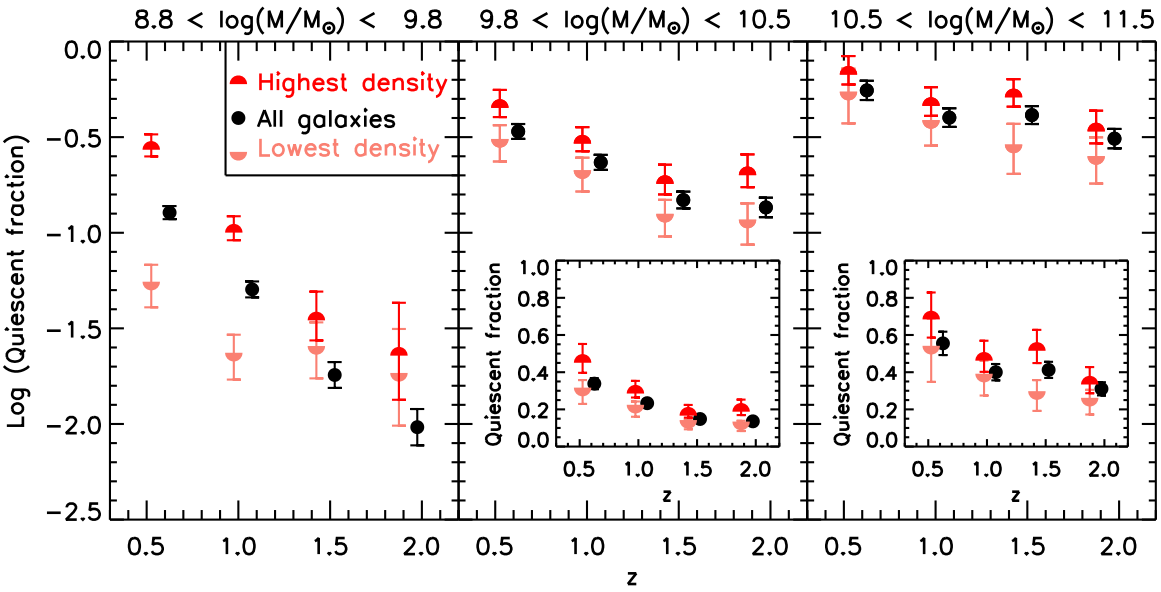

Figure 6. Quiescent fraction vs. redshift in three different stellar mass ranges for all galaxies (black circles), galaxies in the highest-density quartile (red upper-half circles), and galaxies in the lowest-density quartile (light-red lower-half circles). The quiescent fraction of galaxies is determined in bins of $\Delta z = 0.45$, chosen as a balance between redshift sampling and having sufficient statistics in each bin. The error bars indicate 1σ uncertainties based on Poisson statistics. The quiescent fractions of all galaxies (black circles) are slightly offset along the abscissa for clarity. We find a higher quiescent fraction in denser environments for all stellar mass bins out to $z \sim 2.0$, except for the lowest-mass galaxies at $z > 1.5$. Quiescent fractions are shown in log scale to present relative quiescent fractions in each stellar mass range. However, the inset plots in the higher redshift panels show linear scaling for clarity.

quenching" in this study; e.g., Dekel & Burkert 2014; Woo et al. 2015; Zolotov et al. 2015; Terrazas et al. 2016).

In contrast, quenching from environmental processes manifests in different ways. One null hypothesis is that environmental quenching has no effect on galaxy morphology. If this is true, then it would suggest that quiescent galaxies in high-density environments (which are affected by quenching processes that correlate with stellar mass and environment; Figure 8) would have different morphologies from quiescent galaxies in low-density environments (which are affected only by mass quenching); instead, their morphologies would be more similar to the star-forming population in dense environments. We test this hypothesis here by comparing the morphological distributions of quiescent and star-forming galaxies in our different environments.

We begin by showing the number of galaxies as functions of stellar mass and projected local density (environment) at $0.5 < z < 1.0, 1.0 < z < 1.5$, and $1.5 < z < 2.0$ as a function of both $\log(1+\delta')_3$ and $\log(M/M_\odot)$ in Figure 10 (top panels). We then show the quiescent fraction of galaxies at the same redshift ranges as a function of both $\log(1+\delta')_3$ and $\log(M/M_\odot)$ in Figure 10 (middle panels). We observe both environmental quenching and mass quenching out to $z \sim 2.0$—the quiescent fraction of galaxies increases with both stellar mass and overdensity as we have shown earlier.

The middle panel of Figure 10 also shows that for massive galaxies with $\log(M/M_\odot) > 10$, the contour of "constant color" (quiescent fraction) goes from nearly vertical at low redshift to nearly horizontal (the high-density regions) at high redshift, demonstrating that we get 50% of quenching from mass quenching and 50% from environmental quenching, even at $z \sim 2$ (in the high-density regions). This finding is consistent with what we have shown in Figure 8.

The bottom panels of Figure 10 show the median Sérsic index of galaxies at $0.5 < z < 1.0$, $1.0 < z < 1.5$, and $1.5 < z < 2.0$ as a function of stellar mass ($\log(M/M_\odot)$) and environment ($\log(1+\delta')_3$). As shown in the middle panels, we find that the distribution of the median Sérsic index closely resembles that of quiescent fractions of galaxies as in previous works (see references above). In this work, we see that these quantities closely track each other remarkably well across the all masses, environments, and redshifts we probe (this can be seen visually in Figure 10). The similarity of the quiescent fraction and Sérsic index distributions is consistent with the picture in which the (stellar) mass quenching is reflecting the quenching processes that are more directly correlated with morphology, such as bulge-building/compacting mechanisms (e.g., Lang et al. 2014; Woo et al. 2015, 2017b; Zolotov et al. 2015; Tacchella et al. 2016a, 2016b; Terrazas et al. 2016).

In addition, it is interesting that quiescence and concentrated morphology (Sérsic index) go together even at high redshift ($z > 1.5$) and for the environmental quenching, indicating that only particular galaxies are susceptible to environmental quenching, and those are the galaxies that already have a high Sérsic index. These galaxies have time to make it into dense environments, or they collapsed early and have concentrated morphologies. At low redshifts, it is different, as the environment affects galaxy star formation independent of the galaxy properties.

There are some indications of deviations from this. As a function of environmental density, for lower-mass galaxies with $\log(M/M_\odot) < 10.2$, there is some indication that the change in quiescent fraction is faster than the change in galaxy Sérsic index (at fixed stellar mass), and this exists at all redshifts. Figure 11 shows the ratio of quiescent fraction to the median Sérsic index of galaxies (f_q/n) in 0.2 dex bins of projected local density. At low masses ($\log(M/M_\odot) < 10.2$; top panels), the plots show that the ratio of f_q/n is roughly constant for densities $\log(1+\delta')_3 \lesssim 0$ at all redshifts, but that the ratio increases at higher overdensity. This is caused by a faster increase in the quiescent fraction while the median Sérsic index remains roughly constant (or increases slower) as a

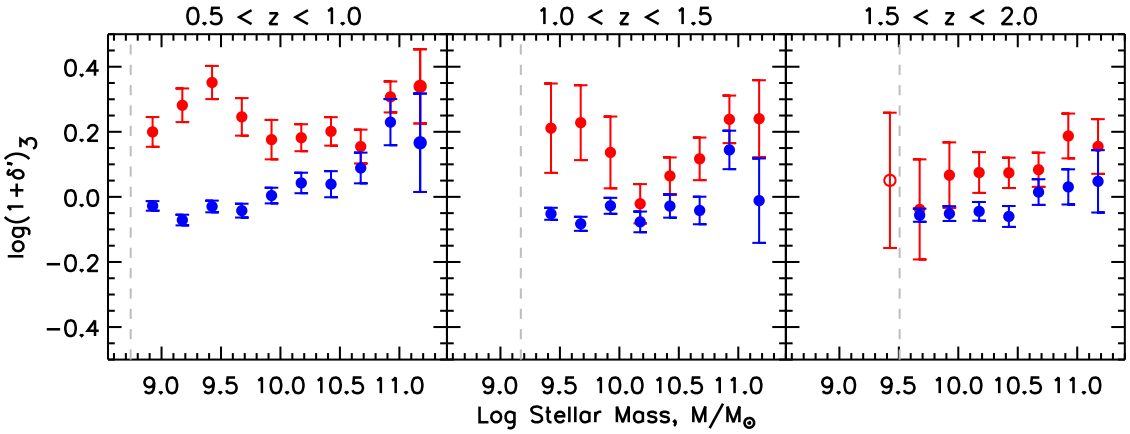

Figure 7. Average overdensity vs. stellar mass for quiescent galaxies (red circles) and star-forming galaxies (blue circles) in 0.25 dex mass bins. The mass completeness at each redshift bin is shown as the vertical dashed line. The error bars are the standard deviation of the mean. Even at fixed mass, the quiescent galaxies tend to have higher overdensities than the star-forming galaxies.

function of projected local density ($\log(1+\delta')_3$) out to $z \sim 2$, at least for these low-mass galaxies (this is evident from a close inspection of Figure 10). Our finding here is consistent with that of Weinmann et al. (2009), who demonstrated that satellite-specific processes mildly enhance the concentration of galaxies once they become satellites. This may be taken as some evidence that these low-mass galaxies retain some memory of the morphology of their star-forming progenitors. However, as we discuss below, once galaxies quench (even as a result of their environment), some process also transforms galaxy morphologies on fast timescales as the distributions of the morphological and structural parameters of quiescent galaxies in high and low densities appear highly similar (see Figure 12).

In contrast, for more massive galaxies ($\log(M/M_{\odot}) > 10.2$; bottom panels of Figure 11), there is no evidence that the ratio of quiescent fraction to the median Sérsic index of these galaxies increases with environmental density. It is also interesting that there are more quiescent high-mass galaxies in dense environments. They already came in with high Sérsic index, providing tentative evidence for a morphological version of the pre-processing—the processes that make galaxies concentrated have happened already.

We compared the morphological properties of the galaxy populations using the cumulative distributions of the Sérsic index (n), effective radius (r_e), axis ratio (b/a) (using values from van der Wel et al. 2012), and stellar mass surface density in the inner 1 kpc ($\Sigma_{1\,\mathrm{kpc}}$) for quiescent and star-forming galaxies in the highest- and lowest-density environments, using the measurements described in Appendix B. At all redshifts and stellar masses in our sample, the quiescent galaxies have higher Sérsic indices, smaller effective radii, higher axis ratios, and higher mass surface densities than star-forming galaxies (Figure 15), in agreement with previous studies both in the local universe (e.g., Bell 2008; Fang et al. 2013; Omand et al. 2014) and at high redshift (e.g., van Dokkum et al. 2011; Wuyts et al. 2011; Barro et al. 2012, 2017; Bell et al. 2012; Cheung et al. 2012; Szomoru et al. 2012; Lang et al. 2014).

Turning to the environmental dependence, we also find that quiescent galaxies in high-density environments have different structural parameters from star-forming galaxies in the same environments. This would not be expected if a significant portion of quiescent galaxies in high-density environments were recently quenched and retained the morphologies of star-forming galaxies. This is true for all subsamples in stellar mass and redshift that we probe, $8.5 < \log(M/M_{\odot}) < 11.0$ and $0.5 < z < 2.0$. Figure 12 shows a summary of the p-values from K–S tests comparing the distributions of quiescent galaxies in the highest -density quartile to those of star-forming galaxies in the highest-density quartile at $0.5 < z < 1.0$, and Appendix B shows the cumulative distributions of the morphological parameters that we tested (Sérsic indexes, effective radii, axis ratios, stellar mass surface densities) for galaxies at the same redshift. We do not show the higher redshift bins, but we find the same results in all bins of mass and redshift. In all cases, the p-values are $\ll 10^{-2}$. In other words, we can reject the hypothesis that their morphologies are drawn from the same parent distribution.

Similarly, there is no evidence (or at best, weak evidence) that quiescent galaxies in high-density environments have different morphologies from quiescent galaxies in low-density environments at any stellar mass or redshift, except at $0.5 < z < 1.0$. At this low redshift, we find tentative evidence that low-mass quiescent galaxies ($8.8 < \log(M/M_{\odot}) < 9.8$) in high-density environments have larger effective radius than their counterparts in low-density environments, and high-mass quiescent galaxies ($\log(M/M_{\odot}) > 10.5$) have higher Sérsic indices than their counterparts in low-density environments. However, the p-values of these are only 0.02 (equivalent to $\sim 2\sigma$ significance under the assumption of a Gaussian distribution). Figure 12 shows a summary of the p-values from K–S tests comparing the distributions of quiescent galaxies in the highest-density quartile to those in the lowest density quartile at $0.5 < z < 1.0$. In all cases, we are unable to reject the hypothesis that the morphological distributions are the same (p-values $> 10^{-1.3}$).

Our results that the morphologies of neither quiescent nor star-forming galaxies depend on environment are generally consistent with previous studies, with some notable exceptions. Some studies have found differences in the sizes and Sérsic indices of galaxies in the (lower-density) field and (higher-density) environments at high redshift, but this has mostly been restricted to comparisons between the field and clusters. Papovich et al. (2012) and Bassett et al. (2013) study the structural and morphological properties of galaxies in a $z = 1.62$ protocluster and compare those with the field galaxies at the same stellar mass and redshift. Both studies show that the cluster quiescent galaxies have larger average effective sizes

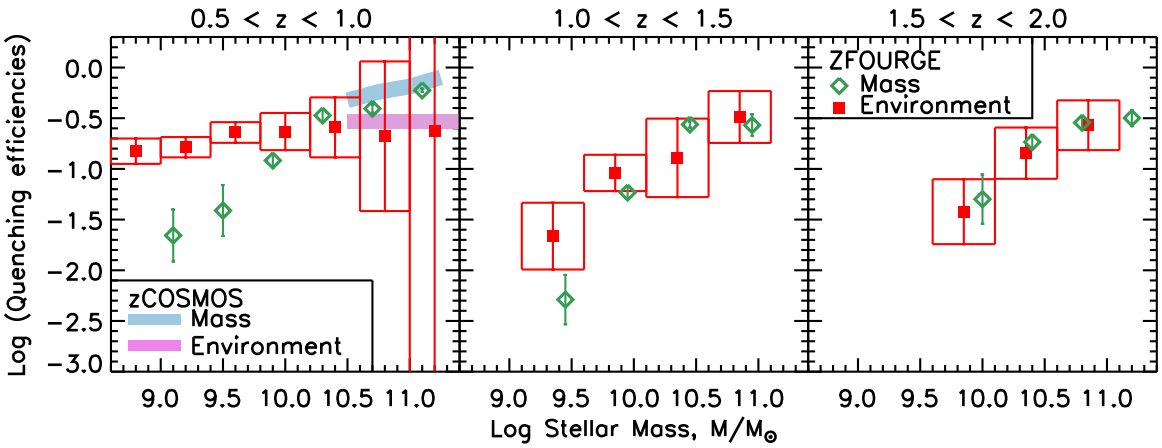

Figure 8. Environmental quenching efficiency (red squares) and (stellar) mass quenching efficiency (green diamond) vs. stellar mass in three different redshift bins. The environmental quenching efficiencies shown here correspond to the highest overdensity quartiles, $\varepsilon_{\rm env}(\delta = \delta_{75}, \delta_0, M)$. The box widths show the stellar mass binning, and the box heights (and error bars) indicate 1σ Poisson uncertainties. The purple and light blue rectangles show the environmental and (stellar) mass quenching efficiencies, respectively, measured in zCOSMOS at $0.3 < z < 0.6$ (Peng et al. 2010). Some error bars are smaller than the size of the data points. The data points are slightly offset for clarity.

compared to field galaxies at fixed mass (see also Cooper et al. 2012; Zirm et al. 2012; Lani et al. 2013; Delaye et al. 2014). In addition, Bassett et al. (2013) found that quiescent cluster galaxies have smaller Sérsic indices compared to the field galaxies (but this was driven by several quiescent galaxies on the edge of the cluster that may be a rare population of recently quenched star-forming galaxies), whereas the star-forming galaxies in both cluster and field show no difference in their morphologies.

On the other hand, Newman et al. (2014) do not detect a significant difference between the mass–radius relation of the quiescent galaxies in the cores of clusters (within $R_{\rm proj} < 1$ pMpc) and quiescent field galaxies at $z \sim 1.8$. Recently, Allen et al. (2016) studied the dependence of the mass–size relation on environment using field and cluster galaxies at $z \sim 1$. The cluster halos of their sample are on the order of $10^{13} M_{\odot}$, which are comparable to the group-sized environments we probe here. Allen et al. ruled out a size difference between quiescent field galaxies and quiescent cluster galaxies. Similarly, they also showed that the Sérsic indices of field quiescent galaxies and cluster quiescent galaxies are consistent. Our results are also consistent with Woo et al. (2017a), who compared the specific SFR–$\Sigma_{1\,\rm kpc}$ relation for field and satellite galaxies from SDSS with stellar mass $\log(M/M_{\odot}) = 9.75$–11.0, and find that, in a given stellar mass bin, quiescent galaxies have higher $\Sigma_{1\,\rm kpc}$ relative to star-forming galaxies by $\sim$0.2–0.3 dex regardless of whether they are field or satellite galaxies. Therefore, our results add to the growing body of literature that the environment at most weakly affects the morphologies of galaxies when matched in mass, star formation activity, and redshift.

The lack of evidence for any environmental dependence of the morphological parameters of star-forming or quiescent galaxies has important consequences for the physical effects that drives environmental quenching. Over the mass and redshift ranges considered here, quiescent galaxies even in high-density environments have very different morphological properties from star-forming galaxies at that epoch, and thus do not appear simply as recently quenched star-forming galaxies. The implication is that the environmental quenching process transforms galaxy morphologies, and it must do so on timescales comparable to the quenching process.

However, it is important to keep in mind the following caveats. We perform the analysis using morphologies as traced by light ("light"-weighted morphology), which may lead to different morphologies as traced by stellar mass ("stellar mass"-weighted morphology Fang et al. 2013). Second, galaxies grow in size with time, but once galaxies are quenched, it stops growing in size at some earlier time. As a result, quiescent galaxies necessarily need to be smaller than star-forming galaxies at a given stellar mass and epoch. Based on this argument, Lilly & Carollo (2016) demonstrated that a high degree of environmental transformation might not be needed if one keeps track of the morphologies of the progenitors of quiescent galaxies and links mild environmental processes, such as stripping of the galaxy's outer part, disk fading, or removal of dust, to reproduce the observed quiescent morphology.

5.3. What Processes Could be Driving Environmental Quenching?

The fact that the environmental quenching efficiency evolves with redshift and (at higher redshift) stellar mass implies that the quenching mechanism itself is correlated with those quantities (namely, time and galaxy stellar mass). This observation is consistent with the "overconsumption" model (McGee et al. 2014), where the environmental quenching time depends on the stellar mass of the satellite. In this model, the cosmological accretion of gas is halted once a galaxy becomes a satellite of a larger halo, and the decline in star formation in satellites is then due to the exhaustion of a gas reservoir through star formation and outflows ("starvation"). The timescale on which the galaxy quenches is equal to the total gas available at the point of accretion, divided by the gas consumption rate.

Given the strong correlation between SFR and stellar mass (e.g., Tomczak et al. 2016), more massive star-forming galaxies have shorter gas-depletion timescales. In the overconsumption model, McGee et al. (2014) predict that delay times should depend both on galaxy stellar mass and redshift. Using this model, Balogh et al. (2016) showed that the high SFRs of

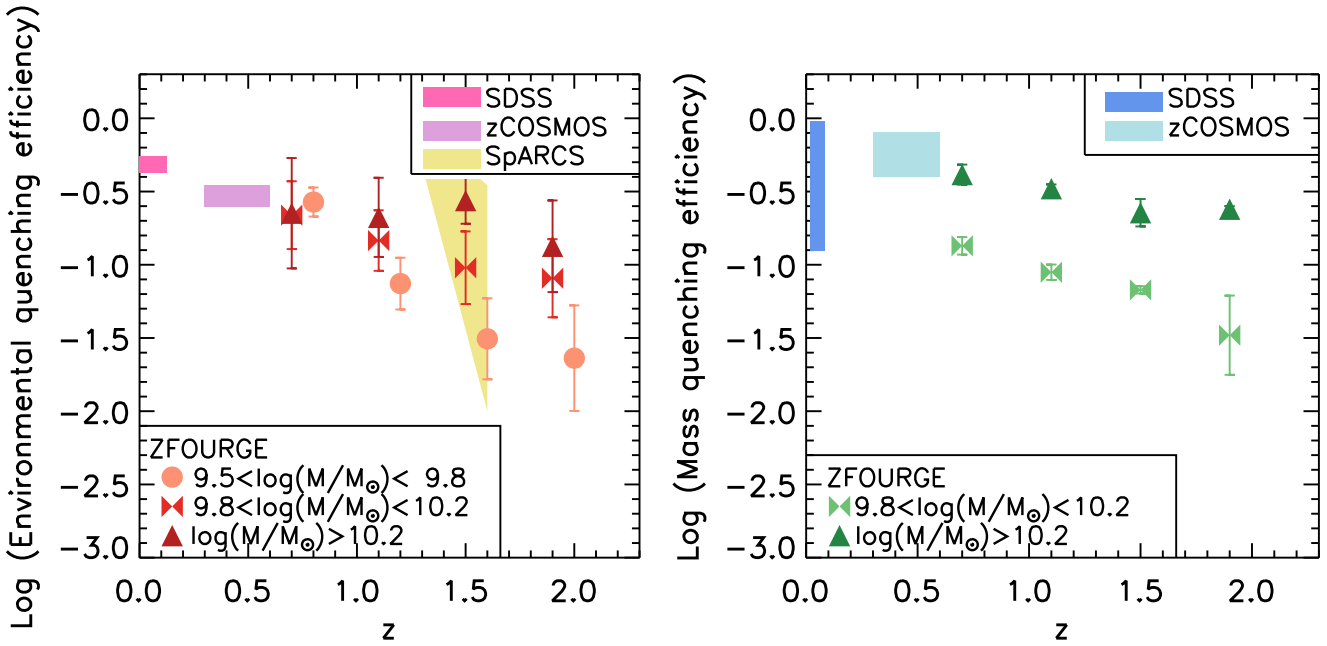

Figure 9. Redshift evolution of the environmental quenching efficiency, $\varepsilon_{\rm env}$, of galaxies in the highest overdensities ($\delta > \delta_{75}$; Equation (4); left panel) and (stellar) mass quenching efficiency ($\varepsilon_{\rm mass}$; Equation (5); right Panel). The different symbols denote the different bins of stellar mass, as labeled. The error bars indicate the 1σ uncertainties based on Poisson statistics. In the left panel, the pink and purple rectangles show the environmental quenching efficiency of galaxies with $9.0 < \log(M/M_{\odot}) < 11.0$ at $0.02 < z < 0.085$ from SDSS and of galaxies with $10.2 < \log(M/M_{\odot}) < 11.0$ at $0.3 < z < 0.6$ from zCOSMOS, respectively (Peng et al. 2010). The yellow-shaded region shows measurements for galaxy clusters at $0.87 < z < 1.63$ with $\log(M/M_{\odot}) > 10.3$ from the *Spitzer* Adaptation of the Red-Sequence Cluster Survey (SpARCS) (Nantais et al. 2016). In the right panel, the filled rectangles show the (stellar) mass quenching efficiency of galaxies with $9.0 < \log(M/M_{\odot}) < 11.0$ at $0.02 < z < 0.085$ from SDSS and of galaxies with $10.2 < \log(M/M_{\odot}) < 11.0$ at $0.3 < z < 0.6$ from zCOSMOS, as labeled (Peng et al. 2010).

massive galaxies ($\log(M/M_{\odot}) \sim 10.5$) in their sample of groups and clusters at high redshift, $0.8 < z < 1.2$, lead to short delay times at $z \sim 1$, consistent with the quenching timescale of at least 3–5 Gyr. This is consistent with the lack of significant environmental quenching of low-mass galaxies at $z > 1$, which we observed here. In addition, McGee et al. argue that, given the strong redshift evolution of the star formation rate, the quenching timescales should be shorter at $z > 1.5$ and is possible even with moderate outflow rates.

Nevertheless, the overconsumption model by itself does not account for the differences in the morphological distributions of the galaxies in our study. Qualitatively, in its simplest form, the overconsumption model predicts no morphological evolution of star-forming galaxies (galaxies simply exhaust their gas supply and retain their morphological appearance at infall modulo the effects of disk fading; see the discussion in Section 5.4 below). Therefore, while overconsumption can mainly account for environmental quenching of a galaxy at high redshift ($z \gtrsim 1$) after it becomes a satellite, it alone probably cannot account for the lack of observed morphological differences in quiescent galaxies in the high- and low-density environments discussed above.

At lower redshift, as galaxy-specific SFRs decline and associated outflow rates decrease, the quenching time predicted from the McGee et al. overconsumption becomes long (>10 Gyr), and other environmental effects that are more closely aligned with dynamical processes in the halo may become more important and ultimately dominate (Balogh et al. 2016). This may also drive the environmental quenching efficiency to be more constant with stellar mass at later times ($z \lesssim 0.5$–1), as is observed here and in previous studies (e.g., Peng et al. 2010; Quadri et al. 2012; Kovač et al. 2014).

At low redshift ($z < 1$), there is still clear evidence that the act of becoming quiescent is accompanied by a change in galaxy structure, and this is true even when environmental processes are responsible for quenching star formation in galaxies. As we discussed above, the environmental quenching processes at low redshift are more likely driven by dynamical processes. Strangulation—the removal of the gas reservoir—is not expected to significantly affect galaxy morphology (see also van den Bosch et al. 2008; Woo et al. 2015). Ram-pressure stripping can remove cold gas from galaxies (e.g., Kenney & Koopmann 1999; Oosterloo & van Gorkom 2005; Chung et al. 2007; Sun et al. 2007; Abramson et al. 2011; Vollmer et al. 2012; Kenney et al. 2015), but again the morphology of a galaxy is not expected to be significantly modified (Weinmann et al. 2006; van den Bosch et al. 2008). Moreover, a hot gaseous halo is a requirement for ram-pressure stripping to be effective in satellites (e.g., Larson et al. 1980; Balogh et al. 2000; Kawata & Mulchaey 2008; McCarthy et al. 2008), so it is not clear that this can be a dominant mechanism in the lower-mass systems that dominate our study.

Although several studies argue that ram-pressure stripping is likely a rapid quenching mechanism, in groups and interacting pairs, it is primarily effective in quenching lower -mass galaxies ($\log(M/M_{\odot}) < 8.0$; Slater & Bell 2014; Davies et al. 2015; Weisz et al. 2015; Fillingham et al. 2016) and is a less relevant quenching mechanism for more moderate-mass galaxies (Woo et al. 2017a, $9.75 < \log M/M_{\odot} < 10$). Given the stellar mass range of galaxies in our samples, their environmental quenching efficiencies, and the expected range of group halo masses (e.g., Fossati et al. 2017), these processes (by themselves) seem unlikely to dominate the overall environmental trends that we observe.

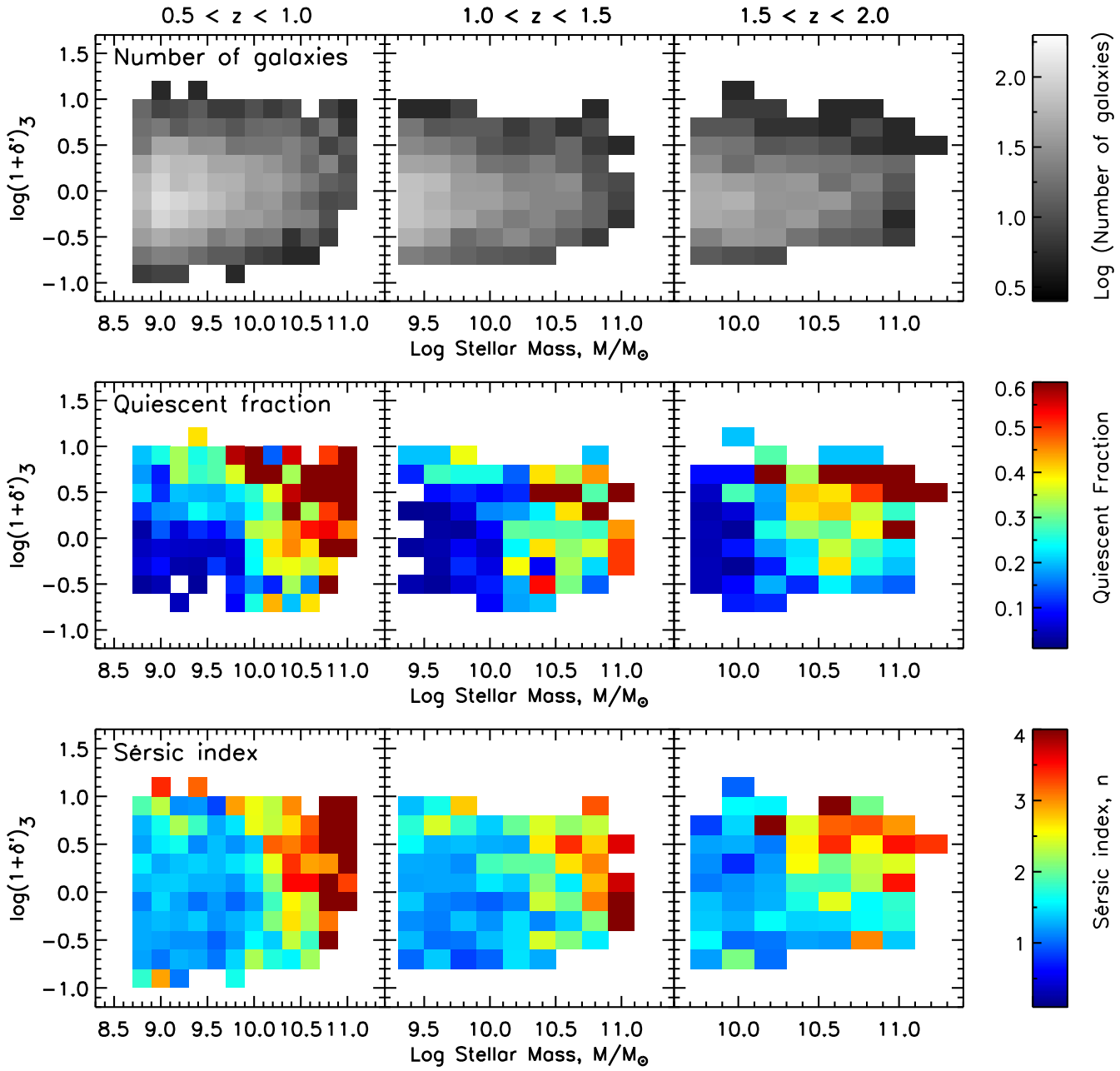

Figure 10. Top: number of galaxies as a function of stellar mass and projected local density (environment) in three redshift bins (from left to right). The number of galaxies is determined in bins of 0.2 dex in both $\log(M/M_{\odot})$ and $\log(1+\delta')$. In each panel, the color-scaling indicates the number of galaxies (as indicated by the color bar); note that the range of the abscissa changes in each panel to include only galaxies down to the stellar mass completeness in each redshift bin. Middle: quiescent fraction of galaxies as a function of stellar mass and projected local density in three redshift bins (from left to right). The quiescent fraction of galaxies is determined in bins of 0.2 dex in both $\log(M/M_{\odot})$ and $\log(1+\delta')$. In each panel, the color-scaling indicates the quiescent fraction (as indicated by the color bar). Bottom: median Sérsic index of galaxies as a function of stellar mass and projected local density for the same redshift bins as in the top panels. The median Sérsic index of galaxies is determined in bins of 0.2 dex in both $\log(M/M_{\odot})$ and $\log(1+\delta')$ as in the top three panels. In each panel, the color-scaling indicates the median Sérsic index (as indicated by the color bar).

5.4. What Processes Could be Driving the Environmental Morphological Transformation?

It may be that multiple environmental processes are at work to quench star-forming galaxies, while others transform their morphologies. One candidate for environmental processes that would affect galaxy morphologies is mergers and interactions (similar to "merging quenching;" Peng et al. 2010), which are expected to be more frequent in denser environments at both $z=0$ and higher redshifts (Fakhouri & Ma 2009). Each merger and interaction can build up the density in the inner kiloparsec of a galaxy (Lake et al. 1998). Such interactions are also shown to be more frequent for higher-mass galaxies out to $z=2.5$ (Xu et al. 2012; Man et al. 2016), where the interactions could increase gas consumption, redistribute angular momentum, and form spheroids.

Frequent galaxy–galaxy encounters also lead to strong tidal torques, which could drive material to galaxy centers, fuel starbursts, build bulges, (e.g., Sobral et al. 2011), and can also lead to disk stripping. These could be combined with disk fading, which enhances the relative importance of the bulge

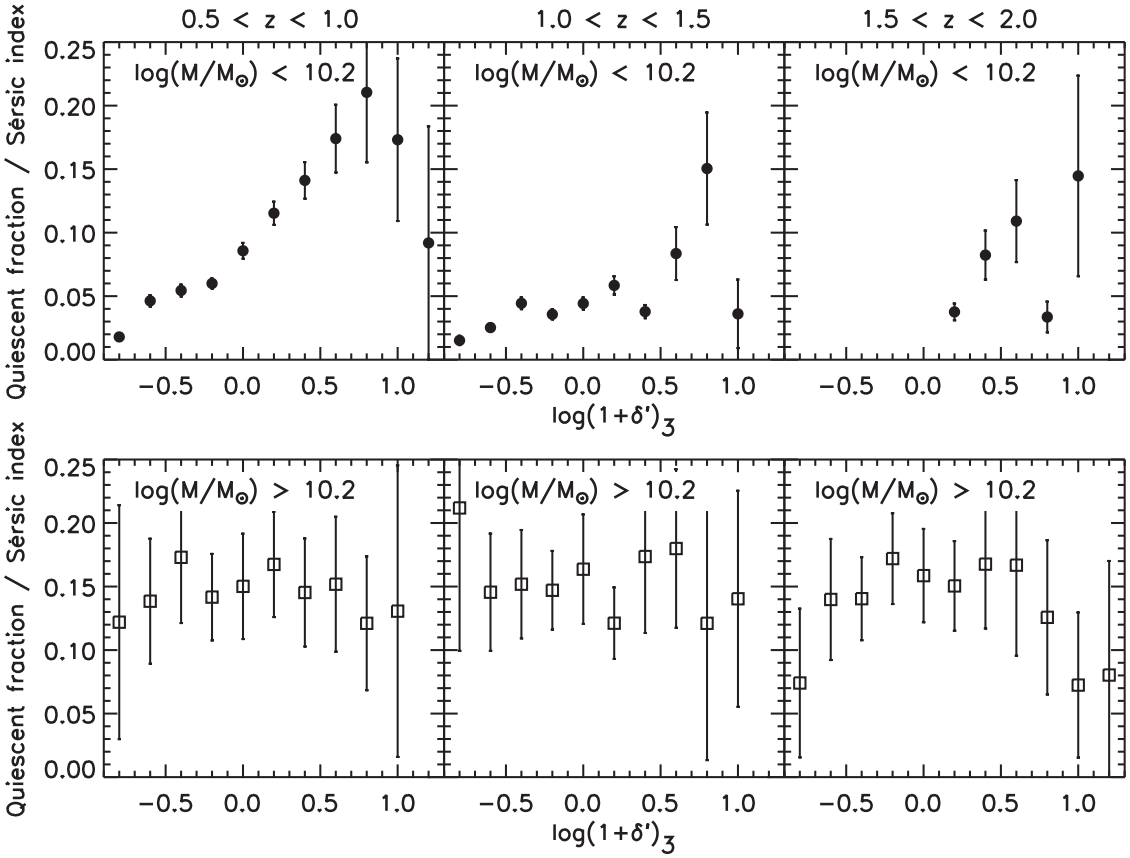

Figure 11. Top: ratio of the quiescent fraction to the median Sérsic index of galaxies (f_q/n) vs. the projected local density (environment) in three redshift bins (from left to right) for $\log(M/M_{\odot}) < 10.2$ galaxies with stellar mass down to the mass-completeness limit in each redshift range. Both quiescent fractions and median Sérsic index of galaxies are determined in bins of 0.2 dex in $\log(1+\delta')$ as in Figure 10. The error bars indicate 1σ uncertainties based on Poisson statistics. Bottom: same as the top panels but for the more massive galaxies ($\log(M/M_{\odot}) > 10.2$).

and shifts the galaxy morphology toward being more bulge dominated (higher Sérsic index and higher $\Sigma_{1\,\mathrm{kpc}}$; e.g., Carollo et al. 2013, 2016). Testing for disk fading requires morphological measurements weighted by stellar mass (rather than weighted by luminosity, which they are at present). For this, we require spatially resolved optical–near-IR structures in galaxies, which will be possible through forthcoming observations with *JWST*. A higher rate of (minor) mergers has been invoked to explain the accelerated morphological evolution in galaxies in higher-density environments (e.g., at $z \sim 1.6$, Papovich et al. 2012; Rudnick et al. 2012; Lotz et al. 2013), and this could explain the weak evidence that massive quiescent galaxies in the highest-density environments have increased Sérsic indices compared to massive quiescent galaxies in low-density environments (based on the *p*-values; Figure 12 and Appendix B). Although these processes act on galaxies over a range of redshift, they also have the ability to transform galaxy morphologies once they become satellites and would help to explain the structural differences in quiescent and star-forming galaxies in different environments.

To summarize, dense galaxy regions are complex environments, and our results suggest that there are multiple processes at work. The redshift and stellar mass evolution of the environmental quenching efficiency favors models where the gas supply is truncated as galaxies become satellites (e.g., starvation), combined with stellar mass-dependent star formation and outflows (e.g., overconsumption). This must be combined with processes such as more frequent interactions and mergers that are prevalent in denser environments and are capable of transforming galaxy morphologies. These processes would naturally connect the quenching timescale with the morphological transformation timescale, which is required to explain the data. This leads to the prediction that massive galaxies in denser environments have more tidal features than those in less dense environments. Again, forthcoming observations with *JWST* will provide deeper imaging to test our prediction.

6. Summary

We studied how the local environmental density affects star formation activity in galaxies using a mass-complete sample to $\log(M/M_{\odot}) > 8.8$–9.5 from the deep near-IR ZFOURGE survey at $z = 0.5$–2.0. We measure galaxy overdensities using a Bayesian-motivated estimate of the distance to the 3NN, where the precise photometric redshifts from ZFOURGE ($\sigma_z/(1+z) \lesssim 0.02$) allow us to measure accurately the galaxies in the highest- and lowest-density environments. We then study the redshift evolution and stellar mass dependence of the quiescent fraction, environmental quenching efficiency, and (stellar) mass quenching efficiency. The main conclusions of this work are the following:

1. The quiescent fraction of galaxies increases in denser environments (greater overdensity). This star-formation–density relation can be traced to at least $z \sim 2.0$ and for galaxies with $\log(M/M_{\odot}) > 9.5$. We show that the star-formation–density relation is not simply the result of a

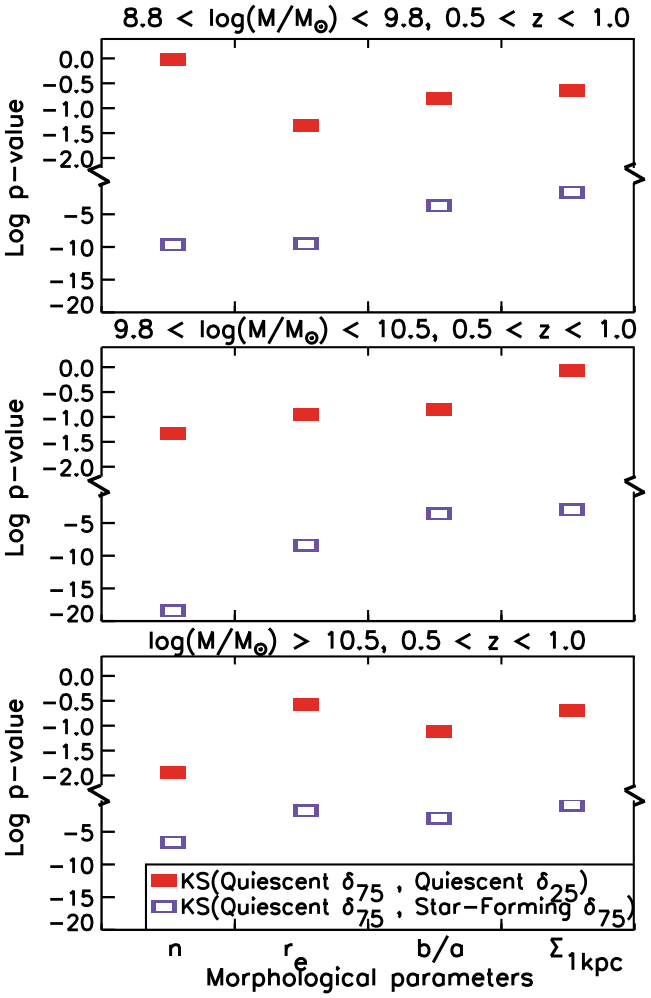

Figure 12. p-values (i.e., likelihoods that the samples have the same parent distribution) from the K–S tests comparing the distributions of four different morphological parameters—Sérsic index (n), effective radius (r_e), axis ratio (b/a), and stellar mass surface density in inner 1 kpc ($\Sigma_{1\,\mathrm{kpc}}$)—for subsamples of quiescent and star-forming galaxies in different environments. The top, middle, and bottom panels show different bins of stellar mass for galaxies at $0.5 < z < 1.0$ (as labeled; these are typical—we do not show higher redshift bins, but they show similar results). Comparing star-forming and quiescent galaxies in high-density environments (open purple rectangles), in all cases the p-values ($\lesssim 10^{-3}$) indicate that we can reject the hypothesis that their morphologies are drawn from the same parent distribution. Performing a similar analysis by comparing quiescent galaxies in the highest-density environments to those in the lowest-density environments (filled red rectangles), the p-values indicate that both populations are drawn from the same parent distribution (all p-values are >0.05), except for the effective radius distributions of low-mass quiescent galaxies and Sérsic index distributions of high-mass quiescent galaxies, but the p-values are only 0.02 (see Sections 2.4 and 5.2 for the discussion).

mass–density relation combined with a mass–star-formation relation: even at fixed mass, there is a higher quiescent fraction of galaxies in denser environments, although the significance of this effect is weaker at $z > 1.5$.

2. Both the environmental quenching efficiency and the (stellar) efficiency evolve with redshift. We observe minimal environmental effects at $z \gtrsim 1.5$ ($\lesssim$5%) for low-mass galaxies ($\log(M/M_\odot) < 9.5$), but the strength of environmental quenching increases at later times, eventually dominating over the mass quenching process, particularly at these lower stellar masses.

   For more massive galaxies ($\log(M/M_\odot) > 9.5$), the environmental quenching efficiency is already significant at high redshift: at $z \sim 2$, it is already ~30% in the highest densities and remains roughly constant as a function of redshift to $z \sim 0$. For these massive galaxies, (stellar) mass quenching and environmental quenching are comparable in high-density environments.
3. The environmental quenching efficiency depends on stellar mass at high redshift, $z > 1$, and the effects of (stellar) mass quenching and environmental quenching are not separable. The environmental quenching mechanisms, particularly for lower-mass galaxies, may be fundamentally different at low and high redshifts. At high redshift, the (stellar) mass dependence of environmental quenching is qualitatively consistent with a decline in star formation due to the exhaustion of a gas reservoir through star formation and outflows in the absence of cosmological accretion (overconsumption). On the other hand, this overconsumption process is less efficient at low redshift, suggesting that an external gas-stripping process like strangulation may become more important.
4. The distribution of galaxy morphology as a function of galaxy star formation activity shows no strong dependence (or at most a weak dependence) on environment. We find an established relation between star formation and morphology such that quiescent galaxies have higher Sérsic indices, smaller effective radii, higher axis ratios, and higher mass surface density than mass-matched samples of star-forming galaxies. We do not detect any strong environmental effect on the morphologies of quiescent galaxies (and similarly for star-forming galaxies). There is the weakest of evidence that at $0.5 < z < 1.0$ in the highest-density environments quiescent massive galaxies have larger Sérsic indices and quiescent lower-mass galaxies have larger effective radii than mass-matched quiescent galaxies in low-density environments, but the evidence is minimal (≈ 1.5–2σ), and these conclusions are tentative.

   The morphologies suggest that environmental quenching must also transform galaxy morphologies such that there is no observable difference with the galaxies in the field. This is true even for the lowest-mass galaxies ($\log(M/M_\odot) = 8.8$) where we expect approximately all such quiescent galaxies to be quenched by their environment. Therefore, the environmental process responsible for quenching the galaxies also transforms their morphologies such that they no longer share the same parent distribution as the mass-matched star-forming galaxies.

We argue that the redshift evolution of the mass and environmental quenching favors models that combine "starvation" (as galaxies become satellites in larger-mass halos) with the exhaustion of a gas reservoir through star formation and outflows ("overconsumption"). These models must be combined with additional processes such as galaxy interactions, tidal stripping, and disk fading to account for the morphological differences between the quenched and star-forming low-mass galaxy populations.

We wish to thank our collaborators in the ZFOURGE and CANDELS teams for their dedication and assistance, without which this work would not have been possible. We also thank the anonymous referee for a very constructive and helpful

report. This work is supported by the National Science Foundation through grants AST 1413317 and 1614668. This work is based on observations taken by the CANDELS Multi-Cycle Treasury Program with the NASA/ESA *HST*, which is operated by the Association of Universities for Research in Astronomy, Inc., under NASA contract NAS5-26555. This work is supported by *HST* program number GO-12060. Support for program number GO-12060 was provided by NASA through a grant from the Space Telescope Science Institute, which is operated by the Association of Universities for Research in Astronomy, Incorporated, under NASA contract NAS5-26555. We acknowledge generous support from the Texas A&M University and the George P. and Cynthia Woods Institute for Fundamental Physics and Astronomy. L.K. thanks the LSSTC Data Science Fellowship Program; her time as a Fellow has benefited this work. G.G.K. acknowledges the support of the Australian Research Council through the award of a Future Fellowship (FT140100933). K.-V.H.T. acknowledges support by the National Science Foundation under grant #1410728.

Appendix A
Measuring Galaxy Overdensities with Photometric Redshifts

In this work, we use a variation of the distance to the 3NN as a measure of the galaxy environment. We derive the 3NN from the ZFOURGE photometric redshifts and here we quantify how well the overdensity derived from the 3NN reproduces the true overdensity as measured in spectroscopic redshift surveys.

We use a mock galaxy catalog based on the semi-analytic model from Henriques et al. (2015), which is the Munich galaxy formation model updated with the *Planck* first-year cosmology. Henriques et al. modify the treatment of baryonic processes to address the overabundance of low-mass galaxies and quiescent galaxies. For our purposes, the details of galaxy formation and feedback in the mock catalog are less important than the actual redshifts (which include both the cosmological expansion and peculiar velocity). We take all galaxies in the mock catalog down to the stellar mass limit of our ZFOURGE survey at every redshift. We then perturb the redshift from the mock catalog by a random number selected from a normal distribution with σ_z equal to the uncertainty of the ZFOURGE photometric redshift ($\sigma_z = 0.01(1+z)$ to $0.02(1+z)$, depending on the galaxy mass and magnitude; see Straatman et al. 2016).

We then calculate the distance to the Nth nearest neighbor, with $N = 1, 2, 3, \ldots, 7$ in two ways. First, we use the "true" redshifts from the mock (which include the peculiar velocity) to measure the distance to the nearest neighbor within a cylindrical volume of length (in the radial dimension) corresponding to $\Delta v = \pm 2100$ km s^{-1}, which serves as an estimate of the density measured in a spectroscopic survey. We then repeat the measurement, but using the perturbed redshifts as an estimate of the density measured by a ZFOURGE-like photometric-redshift survey.

We then compute two estimates of the local surface density of galaxies derived from the Nth nearest neighbor. First, we compute it with the standard method, $\Sigma_N = N(\pi d_N^2)^{-1}$, where d_N is the distance to the Nth nearest neighbor. Second, we use the Bayesian-motivated estimate of the local surface density derived to the Nth nearest neighbor, Σ_N', which uses the density information of the distances to all neighbors $\leqslant N$ (Ivezić et al. 2005; Cowan & Ivezić 2008) defined in Equation (3) above. From both estimates of the local surface density, we compute the overdensity, $(1+\delta)_N$, using Equation (2) above.

For convenience, we define $\log(1+\delta')_N$ $[z_{\rm phot}]$ as the density measured for galaxies in the mock catalog using the ZFOURGE-like photometric-redshift uncertainties. We also define $\log(1+\delta')_N$ $[z_{\rm spec}]$ as the density measured in the mock catalog using "true" redshifts (which include the cosmological and peculiar redshift in the mock catalog). Figure 13 shows the overdensities for the Bayesian 3NN for the mock catalog, $\log(1+\delta')_{N=3}[z_{\rm spec}]$, compared to those derived from the photometric redshifts, $\log(1+\delta')_{N=3}[z_{\rm phot}]$. The relations are clearly correlated, with galaxies at low and high overdensity in the spectroscopic survey generally displaying low and high overdensity when measured in the ZFOURGE-like survey. However, there are clear examples of mismatch; for example, there is a tail of objects with low overdensity, as defined in the spectroscopic-quality data, that have measured high overdensity in the ZFOURGE-like data. This tail is caused by redshift errors and chance projections of unassociated objects along the line of sight and is consistent with the findings of Cooper et al. (2005) that photometric redshifts can wash out structure.

To quantify the accuracy of the overdensity as measured by the ZFOURGE-like data set, we first measured Spearman's correlation coefficient for the overdensities measured in the spectroscopic-like and ZFOURGE-like data sets for the overdenstiy calculated using the $N =$ 2nd, 3rd, 5th, and 7th nearest neighbor, for the standard and Bayesian methods described above. Figure 14 shows the correlation coefficients as a function of N for the mock galaxies. We find that for all redshift bins from $z = 0.5$ to 2.0, the Bayesian density estimators have higher Spearman's correlation coefficient relative to the traditional nearest neighbors regardless of number of nearest neighbors, indicating that the Bayesian density estimator is better correlated with the spectroscopic density estimator relative to the standard Nth nearest neighbors. The two-sided significance (p-value) of the Spearman's correlation coefficient for all three redshift bins are zero, implying very strong correlation. Second, we find that the correlation increases with lower Nth nearest neighbors.

Second, we computed the completeness and contamination in the low- and high-density environments derived using the ZFOURGE-like mock survey. Our goal is to derive robust samples of galaxies in low-density (high-density) environments that are relatively "pure" in that they have a low contamination fraction of galaxies in high-density (low-density) environments misclassified by our method. Specifically, we will define samples of galaxies in high-density and low-density environments based on the ranked quartiles computed using a spline linear regression implemented with the cobs package as we did for our analysis of the ZFOURGE galaxy sample (where we define galaxies in the top density quartile as "high density" and those in the bottom density quartile as "low density.")

Selecting galaxies in the top (highest) density quartile in $\log(1+\delta')_N$ $[z_{\rm phot}]$ using the 3NN ($N = 3$), we recover >80% of galaxies that are also in the top density quartile in $\log(1+\delta')_N$ $[z_{\rm spec}]$ (see Figure 13; the completeness declines for higher values of N). Of the galaxies in the top density quartile in $\log(1+\delta')_N$ $[z_{\rm spec}]$ that we miss, more than half are in the next (third) quartile in $\log(1+\delta')_N$ $[z_{\rm phot}]$. More importantly, the contamination is low. The fraction of galaxies in our top density quartile in $\log(1+\delta')_N$ $[z_{\rm phot}]$ that are actually in the lowest or second-lowest density quartiles in

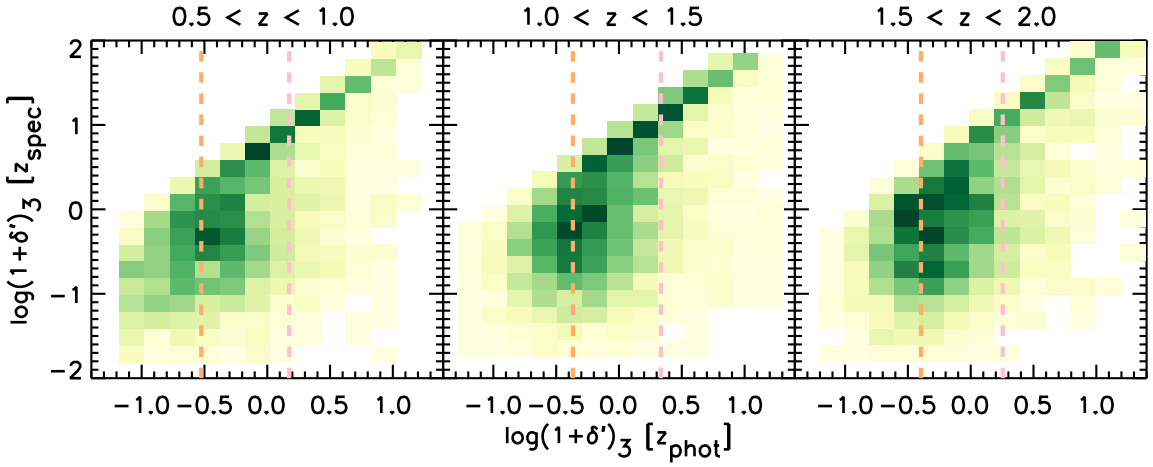

Figure 13. Simulated density measurements based on photometric redshifts ($\log(1+\delta')_{N=3}$ [$z_{\rm phot}$]; $\Delta z = 0.02(1+z)$) vs. measurements based on spectroscopic redshifts ($\log(1+\delta')_{N=3}$ [$z_{\rm spec}$]; $\Delta v = 2100$ km s^{-1}) for the Bayesian-motivated $N = 3$ (third nearest neighbor, 3NN) in three redshift ranges. The orange and pink vertical dashed lines indicate the lowest and top quartiles (the 25th and 75th percentiles of the $\log(1+\delta')_{N=3}$[$z_{\rm phot}$] distribution), which we used to specify low- and high-density environments. There is a strong correlation between both density measurements—at all redshifts, galaxies identified in the highest- (lowest-) density quartiles using photometric redshifts with this precision recover those galaxies in the highest- (lowest-) density quartiles as defined using spectroscopic redshifts.

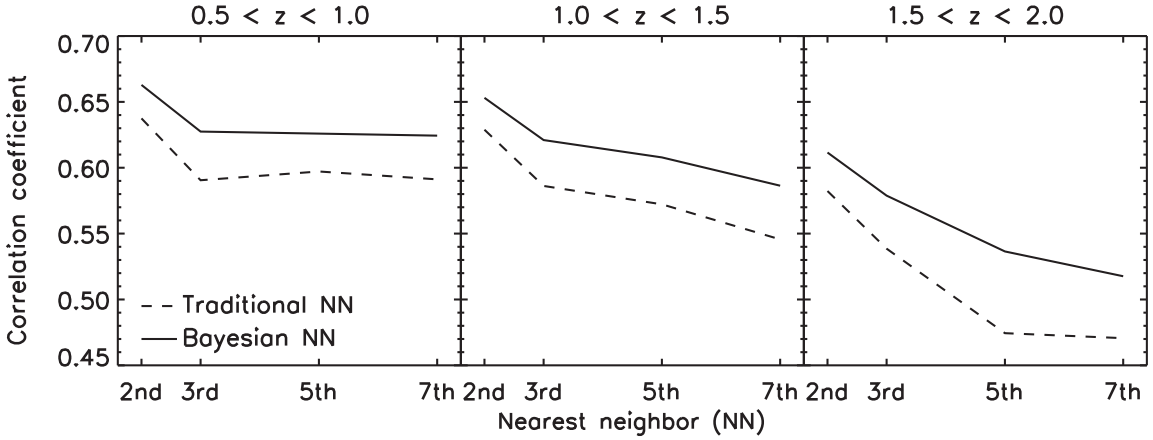

Figure 14. Spearman's correlation coefficient between photometric environment measurements and spectroscopic environment measurements as a function of the Nth nearest neighbors with $N = 2, 3, 5, 7$ for the mock galaxy sample at $0.5 < z < 1.0$ (left), $1.0 < z < 1.5$ (middle), and $1.5 < z < 2.0$ (right). The Bayesian-motivated and traditional Nth nearest neighbors are shown as solid and dashed lines, respectively.

$\log(1+\delta')_N$ [$z_{\rm spec}$] is ~15% (using $N = 3$, i.e., the 3NN; the contamination increases for larger choices of N and also increases when using the non-Bayesian estimator for the nearest neighbor distance). This is acceptable as our goal is to identify a relatively pure sample of galaxies in high-density environments, which we achieve. In other words, we lose about one-third of galaxies that should be in our top density quartile, but the majority (>85%) of galaxies in our top density quartile are truly in high-density environments as measured by $\log(1+\delta')_N$ [$z_{\rm spec}$] (i.e., there is a low incidence of chance alignments of galaxies in projection compared to real, physically associated galaxies).

Selecting galaxies in the bottom (lowest) density quartile in $\log(1+\delta')_N$ [$z_{\rm phot}$], we recover ~80% of galaxies that are also in the lowest-density quartile in $\log(1+\delta')_N$ [$z_{\rm spec}$] for $N = 3$ (see Figure 13). (As for galaxies in high-density environments, we find the completeness decreases for higher N and when using the non-Bayesian estimator for the nearest neighbor distance.) The sample of galaxies in the lowest-density quartile measured by $\log(1+\delta')_N$ [$z_{\rm phot}$] is very pure in that it contains almost no contamination of galaxies in high-density environments in $\log(1+\delta')_N$ [$z_{\rm spec}$] (see Figure 13): we find that the contamination of sources that are in (from the spectroscopic redshift survey) the highest density or second-highest density quartile is 15% (the contamination again increases for larger values of N and when using the non-Bayesian estimator for the nearest neighbor distance). Again, this is acceptable as it says that the majority (80%) of galaxies identified in our lowest-density quartile in $\log(1+\delta')_N$ [$z_{\rm phot}$] are in low-density environments.

Taking the information about the correlation coefficients, completeness, and contamination together, this provides justification that the overdensity derived from the Bayesian 3NN density estimator accurately recovers galaxies in high and low densities with a strong correlation between measured density and true density. We also choose the $N =$ 3rd nearest neighbor as it allows higher completeness and lower contamination (see above). A further advantage of using the 3NN as a density indicator is that it has also been shown to provide a faithful measure of the local environment on scales of galaxy and galaxy group halos, which are appropriate for our study here (Muldrew et al. 2012). Therefore, we adopt the Bayesian 3NN as our density measure for the study here.

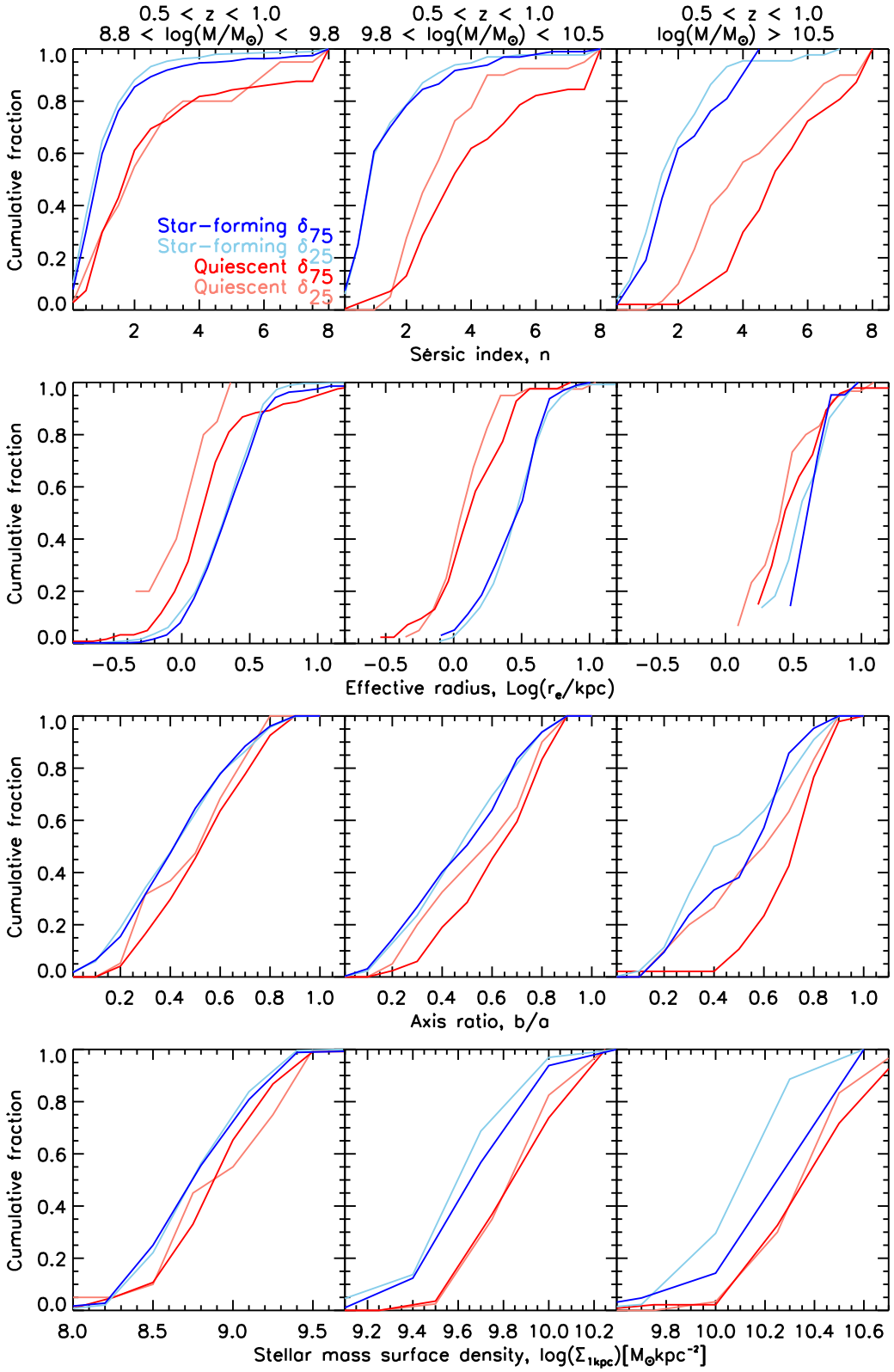

Figure 15. Cumulative distribution of Sérsic index (top row), effective radius (second row), axis ratio (third row), and stellar mass surface density in the inner 1 kpc (bottom row) for quiescent galaxies in the lowest-density quartile (δ_{25}; light-red), quiescent galaxies in the highest-density quartile (δ_{75}; red), star-forming galaxies at $0.5 < z < 1.0$ in the lowest-density quartile (δ_{25}; light blue), and star-forming galaxies in the highest-density quartile (δ_{75}; blue) in three stellar mass ranges. There is no significant evidence for a difference in the distributions of any of the four morphological parameters between quiescent (and star-forming) galaxies in low- and high-density environments, except for the effective radius distributions of low-mass quiescent galaxies and Sérsic index distributions of high-mass quiescent galaxies, but only at the 2σ level of significance (see Section 5.2 for the discusssion).

Appendix B
Stellar Mass Surface Density in the Inner 1 kpc and Cumulative Distributions of Structural Morphological Parameters

In addition to comparing the three morphological parameters, Sérsic index, effective semimajor axis, axis ratio (described in Section 2.4) of quiescent and star-forming galaxies in low- and high-density environments, we also consider correlations with the stellar mass surface density within the inner 1 kpc, $\Sigma_{1\,\mathrm{kpc}}$. We calculate $\Sigma_{1\,\mathrm{kpc}}$ following the procedure described by Bezanson et al. (2009) and Whitaker et al. (2017) using the galaxies' best-fit Sérsic indices (n) and circularized effective radii (r_{eff}). In brief, we assume isotropic spherical galaxies with surface luminosity profiles following the Sérsic profile to perform an Abel transform to deproject the circularized, three-dimensional light profile:

$$\rho\left(\frac{r}{r_e}\right) = \frac{b_n}{\pi}\frac{I_o}{r_e}\left(\frac{r}{r_e}\right)^{1/n-1} \times \int_1^\infty \frac{\exp[-b_n(r/r_e)^{1/n}t]}{\sqrt{t^{2n}-1}}dt. \quad (6)$$

We convert the total luminosity to total stellar mass, assuming that mass follows the light, and that there are no strong color gradients. We follow van Dokkum et al. (2014) by applying a small correction to these stellar masses to take into account the difference between the total magnitude in the photometric catalog and the total magnitude implied by the Sérsic fit (see Taylor et al. 2010). Finally, we calculate the stellar mass surface density in the inner 1 kpc by numerically integrating the following equation:

$$\Sigma_{1\,\mathrm{kpc}} = \frac{\int_0^{1\,\mathrm{kpc}}\rho(r)r^2dr}{\int_0^\infty \rho(r)r^2dr}\frac{L_{\mathrm{model}}}{L_{\mathrm{phot}}}\frac{M_{\mathrm{phot}}}{\frac{4}{3}(1\,\mathrm{kpc})^3}, \quad (7)$$

where M_{phot} is the stellar mass of the galaxy from the ZFOURGE catalogs, L_{phot} is the total, aperture-corrected luminosity from the ZFOURGE catalogs in the bandpass corresponding to the Sérsic profile measurement (H_{160}), and L_{model} is the total luminosity as measured from integrating the best-fit Sérsic profile.

Figure 15 shows the cumulative distributions of the Sérsic index (n), effective radius (r_e), axis ratio (b/a), and stellar mass surface density in the inner 1 kpc ($\Sigma_{1\,\mathrm{kpc}}$) for quiescent galaxies and star-forming galaxies at $0.5 < z < 1.0$ in the lowest and highest overdensity quartiles for three stellar mass bins. In all cases, we find that there is no statistical difference in the distributions of quiescent galaxies in high-density and low-density environments. Similarly, we find that the morphology distributions of star-forming galaxies and quiescent galaxies in the highest-density regions are dissimilar (therefore, quiescent galaxies in high-density regions do not have the morphologies of (recently quenched) star-forming galaxies). We use these distributions in Section 5.2 (see also Figure 12). Note that we do not show our higher redshift bins in the figures, but we find the same results in all bins of mass and redshift.

ORCID iDs

Lalitwadee Kawinwanichakij https://orcid.org/0000-0003-4032-2445
Casey Papovich https://orcid.org/0000-0001-7503-8482
Ryan F. Quadri https://orcid.org/0000-0003-0341-8827
Karl Glazebrook https://orcid.org/0000-0002-3254-9044
Rebecca J. Allen https://orcid.org/0000-0002-7278-9528
Eric F. Bell https://orcid.org/0000-0002-5564-9873
Avishai Dekel https://orcid.org/0000-0003-4174-0374
Henry C. Ferguson https://orcid.org/0000-0001-7113-2738
Ben Forrest https://orcid.org/0000-0001-6003-0541
Norman A. Grogin https://orcid.org/0000-0001-9440-8872
Yicheng Guo https://orcid.org/0000-0003-2775-2002
Anton M. Koekemoer https://orcid.org/0000-0002-6610-2048
Ray A. Lucas https://orcid.org/0000-0003-1581-7825
Themiya Nanayakkara https://orcid.org/0000-0003-2804-0648
Lee R. Spitler https://orcid.org/0000-0001-5185-9876
Caroline M. S. Straatman https://orcid.org/0000-0001-5937-4590
Kim-Vy H. Tran https://orcid.org/0000-0001-9208-2143
Adam Tomczak https://orcid.org/0000-0003-2008-1752

References

Abadi, M. G., Moore, B., & Bower, R. G. 1999, MNRAS, 308, 947
Abramson, A., Kenney, J. D. P., Crowl, H. H., et al. 2011, AJ, 141, 164
Allen, R. J., Kacprzak, G. G., Glazebrook, K., et al. 2016, ApJ, 826, 60
Baldry, I. K., Balogh, M. L., Bower, R. G., et al. 2006, MNRAS, 373, 469
Baldry, I. K., Glazebrook, K., Brinkmann, J., et al. 2004, ApJ, 600, 681
Balogh, M., Eke, V., Miller, C., et al. 2004, MNRAS, 348, 1355
Balogh, M. L., McGee, S. L., Mok, A., et al. 2016, MNRAS, 456, 4364
Balogh, M. L., Morris, S. L., Yee, H. K. C., Carlberg, R. G., & Ellingson, E. 1997, ApJL, 488, L75
Balogh, M. L., Navarro, J. F., & Morris, S. L. 2000, ApJ, 540, 113
Barro, G., Faber, S. M., Koo, D. C., et al. 2017, ApJ, 840, 47
Barro, G., Faber, S. M., Perez-Gonzalez, P. G., et al. 2012, ApJ, 765, 104
Bassett, R., Papovich, C., Lotz, J. M., et al. 2013, ApJ, 770, 58
Bell, E. F. 2008, ApJ, 682, 355
Bell, E. F., van der Wel, A., Papovich, C., et al. 2012, ApJ, 753, 167
Bezanson, R., van Dokkum, P. G., Tal, T., et al. 2009, ApJ, 697, 1290
Birnboim, Y., & Dekel, A. 2003, MNRAS, 345, 349
Birnboim, Y., Dekel, A., & Neistein, E. 2007, MNRAS, 380, 339
Blanton, M. R., & Moustakas, J. 2009, ARA&A, 47, 159
Bower, R. G., Benson, A. J., Malbon, R., et al. 2006, MNRAS, 370, 645
Brammer, G. B., van Dokkum, P. G., & Coppi, P. 2008, ApJ, 686, 1503
Carollo, C. M., Bschorr, T. J., Renzini, A., et al. 2013, ApJ, 773, 112
Carollo, C. M., Cibinel, A., Lilly, S. J., et al. 2016, ApJ, 818, 180
Cattaneo, A., Dekel, A., Devriendt, J., Guiderdoni, B., & Blaizot, J. 2006, MNRAS, 370, 1651
Chabrier, G. 2003, PASP, 115, 763
Cheung, E., Faber, S. M., Koo, D. C., et al. 2012, ApJ, 760, 131
Chung, A., van Gorkom, J. H., Kenney, J. D. P., & Vollmer, B. 2007, ApJL, 659, L115
Chuter, R. W., Almaini, O., Hartley, W. G., et al. 2011, MNRAS, 413, 1678
Cooper, M. C., Coil, A. L., Gerke, B. F., et al. 2010, MNRAS, 409, 337
Cooper, M. C., Griffith, R. L., Newman, J. A., et al. 2012, MNRAS, 419, 3018
Cooper, M. C., Newman, J. A., Coil, A. L., et al. 2007, MNRAS, 376, 1445
Cooper, M. C., Newman, J. A., Madgwick, D. S., et al. 2005, ApJ, 634, 833
Cowan, N. B., & Ivezić, Ž. 2008, ApJL, 674, L13
Croton, D. J., & Farrar, G. R. 2008, MNRAS, 386, 2285
Croton, D. J., Farrar, G. R., Norberg, P., et al. 2005, MNRAS, 356, 1155
Croton, D. J., Springel, V., White, S. D. M., et al. 2006, MNRAS, 365, 11
Cucciati, O., Iovino, A., Kovač, K., et al. 2010, A&A, 524, A2
Cucciati, O., Iovino, A., Marinoni, C., et al. 2006, A&A, 458, 39
Darvish, B., Mobasher, B., Sobral, D., et al. 2016, ApJ, 825, 113
Davies, L. J. M., Robotham, A. S. G., Driver, S. P., et al. 2015, MNRAS, 452, 616
Davies, L. J. M., Robotham, A. S. G., Driver, S. P., et al. 2016, MNRAS, 455, 4013
Davis, M., & Geller, M. J. 1976, ApJ, 208, 13
Dekel, A., & Birnboim, Y. 2006, MNRAS, 368, 2
Dekel, A., & Burkert, A. 2014, MNRAS, 438, 1870
Dekel, A., & Silk, J. 1986, ApJ, 303, 39

Delaye, L., Huertas-Company, M., Mei, S., et al. 2014, MNRAS, 441, 203
Dressler, A. 1980, ApJ, 236, 351
Fakhouri, O., & Ma, C.-P. 2009, MNRAS, 394, 1825
Fang, J. J., Faber, S. M., Koo, D. C., & Dekel, A. 2013, ApJ, 776, 63
Feigelson, E. D., & Babu, G. J. 2012, Modern Statistical Methods for Astronomy (Cambridge: Cambridge Univ. Press)
Fillingham, S. P., Cooper, M. C., Pace, A. B., et al. 2016, MNRAS, 463, 1916
Fillingham, S. P., Cooper, M. C., Wheeler, C., et al. 2015, MNRAS, 454, 2039
Forrest, B., Tran, K.-V. H., Broussard, A., et al. 2017, ApJL, 838, L12
Fossati, M., Wilman, D. J., Mendel, J. T., et al. 2017, ApJ, 835, 153
Franx, M., van Dokkum, P. G., Förster Schreiber, N. M., et al. 2008, ApJ, 688, 770
Gabor, J. M., & Davé, R. 2015, MNRAS, 447, 374
Gabor, J. M., Davé, R., Oppenheimer, B. D., & Finlator, K. 2011, MNRAS, 417, 2676
Geha, M., Blanton, M. R., Yan, R., & Tinker, J. L. 2012, ApJ, 757, 85
Geha, M., Wechsler, R. H., Mao, Y.-Y., et al. 2017, ApJ, 847, 4
Giacconi, R., Zirm, A., Wang, J., et al. 2002, ApJS, 139, 369
Granato, G. L., De Zotti, G., Silva, L., Bressan, A., & Danese, L. 2004, ApJ, 600, 580
Grogin, N. A., Kocevski, D. D., Faber, S. M., et al. 2011, ApJS, 197, 35
Gunn, J. E., & Gott, J. R., III 1972, ApJ, 176, 1
Guo, Y., Bell, E. F., Lu, Y., et al. 2017, ApJL, 841, L22
Hartley, W. G., Conselice, C. J., Mortlock, A., Foucaud, S., & Simpson, C. 2015, MNRAS, 451, 1613
Hatfield, P. W., & Jarvis, M. J. 2016, arXiv:1606.08989
Henriques, B. M. B., White, S. D. M., Thomas, P. A., et al. 2015, MNRAS, 451, 2663
Hogg, D. W., Blanton, M. R., Brinchmann, J., et al. 2004, ApJL, 601, L29
Hogg, D. W., Blanton, M. R., Eisenstein, D. J., et al. 2003, ApJL, 585, L5
Jian, H.-Y., Lin, L., Oguri, M., et al. 2017, arXiv:1704.06219
Kauffmann, G., Heckman, T. M., White, S. D. M., et al. 2003, MNRAS, 341, 54
Kauffmann, G., Li, C., & Heckman, T. M. 2010, MNRAS, 409, 491
Kauffmann, G., Li, C., Zhang, W., & Weinmann, S. 2013, MNRAS, 430, 1447
Kauffmann, G., White, S. D. M., Heckman, T. M., et al. 2004, MNRAS, 353, 713
Kawata, D., & Mulchaey, J. S. 2008, ApJL, 672, L103
Kawinwanichakij, L., Quadri, R. F., Papovich, C., et al. 2016, ApJ, 817, 9
Kenney, J. D. P., Abramson, A., & Bravo-Alfaro, H. 2015, AJ, 150, 59
Kenney, J. D. P., & Koopmann, R. A. 1999, AJ, 117, 181
Kereš, D., Katz, N., Weinberg, D. H., & Davé, R. 2005, MNRAS, 363, 2
Knobel, C., Lilly, S. J., Woo, J., & Kovač, K. 2015, ApJ, 800, 24
Koekemoer, A. M., Faber, S. M., Ferguson, H. C., et al. 2011, ApJS, 197, 36
Kovač, K., Lilly, S. J., Knobel, C., et al. 2010, ApJ, 718, 86
Kovač, K., Lilly, S. J., Knobel, C., et al. 2014, MNRAS, 438, 717
Kriek, M., van Dokkum, P. G., Labbé, I., et al. 2009, ApJ, 700, 221
Lake, G., Katz, N., & Moore, B. 1998, ApJ, 495, 152
Lang, P., Wuyts, S., Somerville, R. S., et al. 2014, ApJ, 788, 11
Lani, C., Almaini, O., Hartley, W. G., et al. 2013, MNRAS, 435, 207
Larson, R. B. 1974, MNRAS, 169, 229
Larson, R. B., Tinsley, B. M., & Caldwell, C. N. 1980, ApJ, 237, 692
Lawrence, A., Warren, S. J., Almaini, O., et al. 2007, MNRAS, 379, 1599
Lee, S.-K., Im, M., Kim, J.-W., et al. 2015, ApJ, 810, 90
Lilly, S. J., & Carollo, C. M. 2016, ApJ, 833, 1
Lin, L., Jian, H.-Y., Foucaud, S., et al. 2014, ApJ, 782, 33
Lotz, J. M., Papovich, C., Faber, S. M., et al. 2013, ApJ, 773, 154
Madau, P., & Dickinson, M. 2014, ARA&A, 52, 415
Man, A. W. S., Zirm, A. W., & Toft, S. 2016, ApJ, 830, 89
McCarthy, I. G., Frenk, C. S., Font, A. S., et al. 2008, MNRAS, 383, 593
McGee, S. L., Bower, R. G., & Balogh, M. L. 2014, MNRAS, 442, L105
Morishita, T., Abramson, L. E., Treu, T., et al. 2017, ApJ, 835, 254
Muldrew, S. I., Croton, D. J., Skibba, R. A., et al. 2012, MNRAS, 419, 2670
Muzzin, A., Wilson, G., Yee, H. K. C., et al. 2012, ApJ, 746, 188
Nanayakkara, T., Glazebrook, K., Kacprzak, G. G., et al. 2016, ApJ, 828, 21
Nantais, J. B., Muzzin, A., van der Burg, R. F. J., et al. 2017, MNRAS, 465, L104
Newman, A. B., Ellis, R. S., Andreon, S., et al. 2014, ApJ, 788, 51
Ng, P., & Maechler, M. 2007, Statistical Modelling, 7, 315
Oemler, A., Jr. 1974, ApJ, 194, 1
Omand, C. M. B., Balogh, M. L., & Poggianti, B. M. 2014, MNRAS, 440, 843
Oosterloo, T., & van Gorkom, J. 2005, A&A, 437, L19
Papovich, C., Bassett, R., Lotz, J. M., et al. 2012, ApJ, 750, 93
Papovich, C., Labbé, I., Quadri, R., et al. 2015, ApJ, 803, 26
Patel, S. G., Holden, B. P., Kelson, D. D., et al. 2012, ApJL, 748, L27
Peng, Y., Lilly, S. J., Kovac, K., et al. 2010, ApJ, 721, 193
Peng, Y., Maiolino, R., & Cochrane, R. 2015, Natur, 521, 192
Phillips, J. I., Wheeler, C., Boylan-Kolchin, M., et al. 2014, MNRAS, 437, 1930
Phillips, J. I., Wheeler, C., Cooper, M. C., et al. 2015, MNRAS, 447, 698
Quadri, R. F., Williams, R. J., Franx, M., & Hildebrandt, H. 2012, ApJ, 744, 88
Read, J. I., Wilkinson, M. I., Evans, N. W., Gilmore, G., & Kleyna, J. T. 2006, MNRAS, 366, 429
Rees, M. J., & Ostriker, J. P. 1977, MNRAS, 179, 541
Rudnick, G. H., Tran, K.-V., Papovich, C., Momcheva, I., & Willmer, C. 2012, ApJ, 755, 14
Schawinski, K., Urry, C. M., Simmons, B. D., et al. 2014, MNRAS, 440, 889
Scoville, N., Aussel, H., Brusa, M., et al. 2007, ApJS, 172, 1
Slater, C. T., & Bell, E. F. 2014, ApJ, 792, 141
Sobral, D., Best, P. N., Smail, I., et al. 2011, MNRAS, 411, 675
Somerville, R. S., Hopkins, P. F., Cox, T. J., Robertson, B. E., & Hernquist, L. 2008, MNRAS, 391, 481
Spitler, L. R., Labbé, I., Glazebrook, K., et al. 2012, ApJL, 748, L21
Springel, V., Di Matteo, T., & Hernquist, L. 2005, MNRAS, 361, 776
Straatman, C. M. S., Spitler, L. R., Quadri, R. F., et al. 2016, ApJ, 830, 51
Strateva, I., Ivezić, Ž, Knapp, G. R., et al. 2001, AJ, 122, 1861
Sun, M., Donahue, M., & Voit, G. M. 2007, ApJ, 671, 190
Szomoru, D., Franx, M., & van Dokkum, P. G. 2012, ApJ, 749, 121
Tacchella, S., Dekel, A., Carollo, C. M., et al. 2016a, MNRAS, 458, 242
Tacchella, S., Dekel, A., Carollo, C. M., et al. 2016b, MNRAS, 457, 2790
Taylor, E. N., Franx, M., Glazebrook, K., et al. 2010, ApJ, 720, 723
Terrazas, B. A., Bell, E. F., Henriques, B. M. B., et al. 2016, ApJL, 830 L12
Tinker, J. L., & Wetzel, A. R. 2010, ApJ, 719, 88
Tomczak, A. R., Quadri, R. F., Tran, K.-V. H., et al. 2016, ApJ, 817, 118
Tran, K.-V. H., Papovich, C., Saintonge, A., et al. 2010, ApJL, 719, L126
van den Bosch, F. C., Aquino, D., Yang, X., et al. 2008, MNRAS, 387, 79
van der Wel, A., Bell, E. F., Haussler, B., et al. 2012, ApJS, 203, 24
van Dokkum, P. G., Bezanson, R., van der Wel, A., et al. 2014, ApJ, 791, 45
van Dokkum, P. G., Brammer, G., Fumagalli, M., et al. 2011, ApJL, 743, L15
Ivezić, Ž, Vivas, A. K., Lupton, R. H., & Zinn, R. 2005, AJ, 129, 1096
Vollmer, B., Soida, M., Braine, J., et al. 2012, A&A, 537, A143
Weinmann, S. M., Kauffmann, G., van den Bosch, F. C., et al. 2009, MNRAS, 394, 1213
Weinmann, S. M., van den Bosch, F. C., Yang, X., & Mo, H. J. 2006, MNRAS, 366, 2
Weisz, D. R., Dolphin, A. E., Skillman, E. D., et al. 2015, ApJ, 804, 136
Wetzel, A. R., Tollerud, E. J., & Weisz, D. R. 2015, ApJL, 808, L27
Whitaker, K. E., Bezanson, R., van Dokkum, P. G., et al. 2017, ApJ, 838, 19
White, S. D. M., & Rees, M. J. 1978, MNRAS, 183, 341
Williams, R. J., Quadri, R. F., Franx, M., van Dokkum, P., & Labbé, I. 2009, ApJ, 691, 1879
Woo, J., Carollo, C. M., Faber, S. M., Dekel, A., & Tacchella, S. 2017a, MNRAS, 464, 1077
Woo, J., Carollo, C. M., Faber, S. M., Dekel, A., & Tacchella, S. 2017b, MNRAS, 464, 1077
Woo, J., Dekel, A., Faber, S. M., et al. 2013, MNRAS, 428, 3306
Woo, J., Dekel, A., Faber, S. M., & Koo, D. C. 2015, MNRAS, 448, 237
Wuyts, S., Förster Schreiber, N. M., van der Wel, A., et al. 2011, ApJ, 742, 96
Xu, C. K., Zhao, Y., Scoville, N., et al. 2012, ApJ, 747, 85
Yuan, T., Nanayakkara, T., Kacprzak, G. G., et al. 2014, ApJL, 795, L20
Zirm, A. W., Toft, S., & Tanaka, M. 2012, ApJ, 744, 181
Zolotov, A., Dekel, A., Mandelker, N., et al. 2015, MNRAS, 450, 2327